



Chem Soc Rev

**Influence of Solvent Structure and Hydrogen Bonding on
Catalysis at Solid-Liquid Interfaces**

Journal:	<i>Chemical Society Reviews</i>
Manuscript ID	CS-SYN-06-2021-000539.R2
Article Type:	Review Article
Date Submitted by the Author:	31-Aug-2021
Complete List of Authors:	Potts, David; University of Illinois at Urbana-Champaign, Department of Chemical and Biomolecular Engineering Bregante, Daniel; University of Illinois at Urbana-Champaign, Department of Chemical and Biomolecular Engineering Adams, Jason; University of Illinois at Urbana-Champaign, Department of Chemical and Biomolecular Engineering Torres, Chris; University of Illinois at Urbana-Champaign, Department of Chemical and Biomolecular Engineering Flaherty, David; University of Illinois at Urbana-Champaign, Department of Chemical and Biomolecular Engineering

SCHOLARONE™
Manuscripts

ARTICLE

Influence of Solvent Structure and Hydrogen Bonding on Catalysis at Solid-Liquid Interfaces

David S. Potts,^a Daniel T. Bregante,^a Jason S. Adams,^a Chris Torres,^a and David W. Flaherty^{a,*}

Received 00th January 20xx,
Accepted 00th January 20xx

DOI: 10.1039/x0xx00000x

Solvent molecules interact with reactive species and alter the rates and selectivities of catalytic reactions by orders of magnitude. Specifically, solvent molecules can modify the free energies of liquid phase and surface species via solvation, participating directly as a reactant or co-catalyst, or competitively binding to active sites. These effects carry consequences for reactions relevant for the conversion of renewable or recyclable feedstocks, the development of distributed chemical manufacturing, and the utilization of renewable energy to drive chemical reactions. First, we describe the quantitative impact of these effects on steady-state catalytic turnover rates through a rate expression derived for a generic catalytic reaction ($A \rightarrow B$), which illustrates the functional dependence of rates on each category of solvent interaction. Second, we connect these concepts to recent investigations of the effects of solvents on catalysis to show how interactions between solvent and reactant molecules at solid-liquid interfaces influence catalytic reactions. This discussion demonstrates that the design of effective liquid phase catalytic processes benefits from a clear understanding of these intermolecular interactions and their implications for rates and selectivities.

1. Introduction to Solvent Effects in Catalysis

Catalysis science has progressed tremendously in understanding reactions over solid surfaces,¹⁻³ homogeneous molecular complexes,⁴⁻⁶ and in complex phases (e.g., plasma,⁷⁻⁹ ionic liquids¹⁰⁻¹¹). Since the earliest reports from Berzelius,¹² the majority of efforts in heterogeneous catalysis involved the investigation and design of active sites with a specific focus on covalent or ionic bonds formed with reactive species and their dependence on apparent properties of the solid catalyst (e.g., metal identity,¹³⁻¹⁴ atomic coordination,¹⁵⁻¹⁶ oxidation state¹⁷⁻¹⁸). The reaction environment, however, also warrants consideration for liquid phase systems. Solvent molecules can influence reaction rates by directly participating in catalytic reactions (e.g., facilitating proton transfer, acting as reactants), influencing the stability of chemical species (e.g., solvating through hydrogen bonds), and reducing the number of active sites that bind reactants (e.g., through competitive adsorption).

Researchers first recognized that solvent molecules affect rates of organic reactions over one century ago. In 1890, Menshutkin found that rates for the quaternization of triethylamine with iodoethane depend strongly on solvent choice, as rates in benzyl alcohol are 700 times greater than in n-hexane holding all other reaction conditions constant.¹⁹ This increase in rates occurs because protic benzyl alcohol molecules stabilize the separation of charges within the transition state for quaternization. Several publications documented the effects of solvents upon homogeneous chemical and catalytic reactions in recent years.²⁰⁻

²¹ Evidently, the field of catalysis recognizes the importance of solvent identity on chemical and catalytic reactions, which motivates the need to understand the variety of roles solvent molecules may hold for catalysis. Multiple analytic models emerged over the last century to describe the interaction of solvent molecules on chemical reactions.

Classical theories, such as from Debye and Hückel,²² Kamlet and Taft,²³ and Kirkwood,²⁴ describe the influence of intermolecular forces on the energy (or thermodynamic activity) of solute molecules as functions of bulk properties of the solvent (e.g., dielectric constant, ionic strength, polarizability). These continuum descriptors provide useful guidance for homogeneous reactions; however, these models do not capture specific interactions at the molecular level (e.g., hydrogen bonds, dative bonds) and implicitly assume the structure of the solvent resembles that of the bulk liquid at all positions within the system. Consequently, these theories cannot account for phenomena that affect catalysis at solid-liquid interfaces. This realization motivated the development of quantitative, molecularly informed conceptual frameworks to gain insight into the structure and dynamics near solid-liquid interfaces.

In recent years, a renaissance of work highlighted new methods to characterize interactions between solvent molecules and reactants at solid-liquid interfaces. Gould and Xu examined the use of modern characterization techniques, such as ATR-FTIR spectroscopy, to understand the role of solvent molecules on catalyst properties (e.g., acidity).²⁵ Sievers et al. reviewed the effect of solvent interactions with reactants and catalysts on reactions at solid-liquid interfaces.²⁶ Harris et al. discussed how solvents together with active site configuration, metal identity, and pore size within zeolites affect catalysis and outlined opportunities to develop further understanding.²⁷ Bates and

^a Department of Chemical and Biomolecular Engineering, University of Illinois at Urbana-Champaign, Urbana, IL 61801, USA. E-mail: dwflhrty@illinois.edu
Electronic Supplementary Information (ESI) available: [details of any supplementary information available should be included here]. See DOI: 10.1039/x0xx00000x

Gounder utilized transition state theory to explain the kinetic implications of solvation and solvent clustering on reactions in Brønsted and Lewis acid catalysts.²⁸ Li et al. described several ways by which water influences reaction rates on heterogeneous catalysts with a discussion of reactant and product solubilities, interphase transport, reactive species stability, and the direct participation of water molecules in catalysis.²⁹ Stanciakova and Weckhuysen also reviewed how water molecules can impact zeolite catalysis by interacting with active sites, reactants, and zeolite framework atoms.³⁰

Herein, we begin by deriving equations that quantify the effect of solvent interactions on reactant free energies. We then discuss how three categories of solvent effects influence activation free energies (ΔG_{app}^\ddagger) and free energies of reactions. *First*, solvent molecules form discrete structures that solvate reactants in the liquid phase, surface-bound intermediates, and transition states. The reorganization of these solvent structures during a catalytic cycle leads to significant changes in the free energy of each state along the reaction coordinate. *Second*, solvent molecules act as reactants or co-catalysts that participate directly by facilitating bond formation or cleavage events through specific chemical interactions (e.g., H-atom shuttling). *Third*, solvent molecules inhibit catalysis by competitively binding to active sites or forming extended networks around active sites, thereby displacing reactive intermediates or blocking reactant accessibility to active sites. These three phenomena significantly affect reaction rates at solid-liquid interfaces by altering the free energy of reactive species and merit consideration in the design or investigation of processes that involve liquid phase chemical reactions (e.g., oxidation of hydrocarbons and oxygenates,³¹ and alkylation or carbon coupling for pharmaceutical production^{21, 32}).

2. Solvent Effects on Free Energies of Reactive Species: Derivation of Rate Expressions

A solvent can affect the free energy of reactants, intermediates, and transition states in ways that influence product formation rates and selectivities without changes to the reaction mechanism.²¹ Simple rate equations can explicitly show the dependence of rates on solvation effects and reflect the contributions for each reactive species.

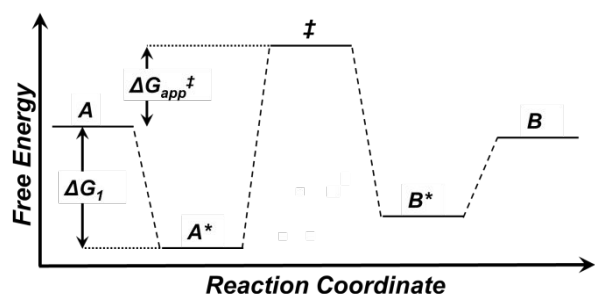
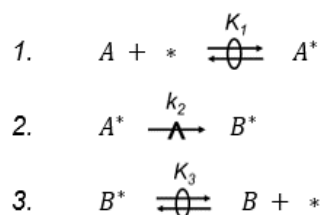


Figure 1. A heterogeneously catalyzed reaction where a single product (B) forms from a single reactant (A). Relevant free energy changes are labelled.

2.1 Derivation for an Ideal Reaction

Let us consider a heterogeneously catalyzed reaction ($A \rightarrow B$) as illustrated in Fig. 1 and Scheme 1:



Scheme 1. Elementary steps for the heterogeneously catalyzed reaction where a single product (B) forms from a single reactant (A). The \rightleftharpoons symbol denotes a quasi-equilibrated step, and the $\xrightarrow{\quad}$ symbol signifies the kinetically relevant step.

The reaction consists of three elementary steps: adsorption of reactant A onto unoccupied active sites (denoted as *), the surface reaction of A^* to form B^* , and the desorption of B^* into the solution to evolve product B. Here, we assume the adsorption and desorption steps are quasi-equilibrated (QE) and the surface reaction that forms B^* is kinetically relevant. All other steps are presumed to reach QE to remove free energy values of intermediates from the equations describing apparent free energies for activation, shown below. While an assumption of QE for these elementary steps greatly simplifies these equations, turnover rates for catalytic reactions depend directly on the free energy of the transition state for a kinetically relevant step (G^\ddagger , Fig. 1) when other preceding or subsequent steps do not reach QE. A balance upon all forms of the active site (i.e., $[L] = [*] + [A^*] + [B^*] + [S^*]$, where $[X^*]$ denotes the number of surface species present) provides an expression for the turnover rate ($r_2/[L]$):

$$\frac{r_2}{[L]} = \frac{k_2 K_1 [A]}{1 + K_1 [A] + K_3^{-1} [B]} \quad (1)$$

where k_2 is the rate constant for step 2, K_1 and K_3 represent equilibrium constants for steps 1 and 3, respectively, and $[A]$ and $[B]$ are liquid phase concentrations of the reactant and product. Eq. 1 represents an ideal reaction in which activity coefficients of all species are equal to unity, and reaction rates are functions of concentrations and related rate and equilibrium constants. Applying transition state theory³³ and assuming that the unoccupied catalytic site is the most abundant reactive intermediate (MARI) (i.e., $1 \gg K_1 [A] + K_3^{-1} [B]$), an apparent rate constant k_{app} can be defined and substituted into the rate expression:

$$k_{app} = k_2 K_1 = \frac{k_B T}{h} K^\ddagger K_1 = \frac{k_B T}{h} \cdot \exp\left(-\frac{\Delta G_{app}^\ddagger}{RT}\right) \quad (2)$$

$$\frac{r_2}{[L]} = \frac{k_B T}{h} \cdot \exp\left(-\frac{\Delta G_{app}^\ddagger}{RT}\right) \cdot [A] \quad (3)$$

where K^\ddagger is the equilibrium constant between the transition state and reference state and ΔG_{app}^\ddagger is the apparent free energy barrier.

2.2 Accounting for Interactions between Reactive Intermediates and Solvents

Interactions between solvent molecules and reactants in the liquid phase and at active sites located at solid-liquid interfaces introduce thermodynamic non-idealities to a catalytic system.³⁴ As a result, K^\ddagger and K_I from Eq. 2 must be described in terms of the activities (a_i) and activity coefficients (γ_i) of reactive species:

$$K^\ddagger = \frac{a^\ddagger}{a_{A^*}} = \frac{\gamma^\ddagger [^\ddagger]}{\gamma_{A^*} [A^*]} \quad (4)$$

$$K_I = \frac{a_{A^*}}{a_A} = \frac{\gamma_{A^*} [A^*]}{\gamma_A [A]} \quad (5)$$

The excess free energy (G^e) quantifies the impact of solvent interactions on the free energy of each component. The activity coefficients of reactive species can be related to excess Gibbs free-energy contributions as follows:

$$\gamma_i = \exp\left(\frac{G_i^e}{RT}\right) \quad (6)$$

The solvent can alter activation barriers and adsorption energies for a reaction when it affects the excess free energies of reactants, intermediates, and transition states to different extents (*Note: throughout this contribution, an increase in G_i^e represents a change where G_i^e becomes more positive; i.e., the species i is destabilized*). These changes lead to differences in rates and selectivities between solvents, even in the absence of mass transfer limitations. The adsorption free energy (ΔG_I) and ΔG_{app}^\ddagger depend upon the standard state (G^0) and excess free energies of the reactant (G_A^e), surface intermediate ($G_{A^*}^e$), and transition state (G^{\ddagger}):

$$\Delta G_I = (G_{A^*}^0 + G_{A^*}^e) - (G_A^0 + G_A^e) \quad (7)$$

$$\Delta G_{app}^\ddagger = (G^{0,\ddagger} + G^{\ddagger,e}) - (G_A^0 + G_A^e) \quad (8)$$

where ΔG_{app}^\ddagger relates to the activation enthalpy (ΔH_{app}^\ddagger) and entropy (ΔS_{app}^\ddagger) as follows:

$$\Delta G_{app}^\ddagger = \Delta H_{app}^\ddagger - T\Delta S_{app}^\ddagger \quad (9)$$

Eq. 8 represents ΔG_{app}^\ddagger for the reaction in Section 2.1 when unoccupied sites comprise the MARI. The terms that provide the value of ΔG_{app}^\ddagger differ under conditions where an adsorbed reactant (A^*) is the MARI. In this case, ΔG_{app}^\ddagger becomes equal to the difference between the free energies of the transition state and surface intermediate A^* :

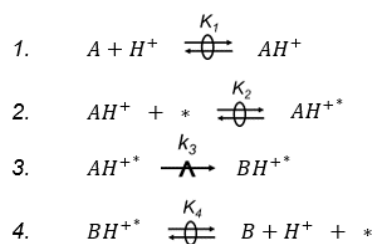
$$\Delta G_{app}^\ddagger = (G^{0,\ddagger} + G^{\ddagger,e}) - (G_{A^*}^0 + G_{A^*}^e) \quad (10)$$

While the excess free energies equal zero for ideal solutions and pure liquids, these terms are non-zero and may be significant within non-ideal solutions and at interfaces. Substituting in terms to Eq. 3 gives a rate expression restated in a manner that includes activity coefficients:

$$\frac{r_2}{[L]} = \frac{k_B T}{h} \cdot \exp\left(-\frac{(G^{0,\ddagger} - G_A^0)}{RT}\right) \cdot \frac{\gamma_A [A]}{\gamma^\ddagger} \quad (11)$$

At solid-gas interfaces, adsorbed species are frequently stabilized through van der Waals interactions with pore walls (e.g., in zeolites³⁵⁻³⁷) or covalent bonds with metal and metal-oxide surfaces.³⁸⁻⁴⁰ The situation differs considerably in the liquid phase. Here, the stability of molecules also depends on non-covalent intermolecular interactions with solvent molecules described by equations of state such as models by Abrams and Prausnitz (universal quasichemical, UNIQUAC),⁴¹ Renon and Prausnitz (non-random two-liquid, NRTL),⁴² and Wilson,⁴³ among others. Interactions with solvent molecules affect the activities of reactive species at solid-liquid interfaces in similar ways. However, the variety and complexity of catalyst surfaces have hindered the development of predictive descriptions for interactions between the extended surface of solid catalysts, surrounding solvent molecules, and reactive species bound to active sites. Relationships that capture these interactions without computationally expensive *ab initio* calculations would provide powerful guidance for catalyst design.

2.3 Direct Participation of Solvent Molecules in Catalysis



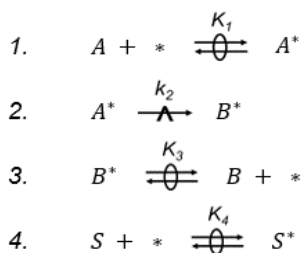
Scheme 2. Elementary steps for the conversion of reactant A to product B, facilitated by a proton from solvent.

A solvent may also participate directly in catalysis. For example, consider the proton-facilitated reaction shown in Scheme 2, with a kinetically relevant surface reaction and all other steps QE. Applying an active site balance gives a rate expression ($r_3/[L]$):

$$\frac{r_3}{[L]} = \frac{k_3 K_1 K_2 [A][H^+]}{1 + K_1 K_2 [A][H^+] + K_4^{-1} [B][H^+]} \quad (12)$$

The rate depends on the pH of the solvent because protons (H^+) from the solution appear directly within the balanced elementary steps. A solvent can also directly facilitate protons and electron transfer between reactants and catalysts, as described by the Grotthuss mechanism.⁴⁴ In doing so, the solvent may introduce reaction pathways not accessible in the absence of solvent. For example, the presence of an aqueous solvent facilitates proton transfer and allows for the formation of 3-cyclohexenone as the final product of phenol hydrogenation, a pathway inaccessible in the vapor phase.⁴⁵

2.4 Rate Inhibition due to Competitive Adsorption of Solvents



Scheme 3. Elementary steps for the liquid phase heterogeneously catalyzed reaction where a single product (B) forms from a single reactant (A) in the presence of a competitively adsorbing solvent.

The solvent may also inhibit catalysis by competitively binding to the active site. Adding a fourth step to the series of elementary steps from Scheme 1 describes a new scenario that includes QE adsorption of solvent molecules to the active site (Scheme 3). The rate expression defined in Eq. 1 then becomes:

$$\frac{r_2}{[L]} = \frac{k_2 K_1 [A]}{1 + K_1 [A] + K_3^{-1} [B] + K_4 [S]} \quad (13)$$

where $K_4[S]$ represents the coverage of solvent molecules on the catalyst surface. Greater solvent coverage decreases the number of available active sites for reactants to adsorb. Defining the solvent as the MARI and introducing additional terms to Eq. 11 gives:

$$\frac{r_2}{[L]} = \frac{k_B T}{h} \cdot \exp\left(-\frac{(G^{0,\ddagger} - G_A^0 - G_{S^*}^0)}{RT}\right) \cdot \frac{\gamma_A [A]}{\gamma_{\ddagger}} \cdot \frac{1}{\gamma_S [S]} \quad (14)$$

in which $G_{S^*}^0$ defines the free energy of solvent molecules adsorbed to the catalyst surface, which must desorb to allow the reactant to adsorb.

The subsequent sections describe specific situations in which one or more of these categories of solvent effects influence rates or selectivities of catalytic reactions upon solid materials or within microporous structures. These examples demonstrate the significance of solvent interactions and show that solvents affect the excess free energy of liquid phase reactants and reactive intermediates and transition states on the catalyst surface through solvation, direct participation in catalysis, and

competitive adsorption. The concise equations derived in this section allow us to deconvolute the energetic effects of these solvent phenomena, identify the specific free energy quantities affected during catalysis at solid-liquid interfaces, and categorize types of solvent effects with the intent to establish connections across a rich body of literature.

3. Solvation of Reactive Species Influence Free Energies, Reaction Rates, and Reaction Pathways

In a condensed phase reaction, the solvent structure around the reactants, intermediates, and transition state differs due to a combination of specific and non-specific intermolecular forces. These various forces thereby affect G^{\ddagger} for each species to different extents, and by extension, can alter reaction rates. First, the properties of zeolites (Section 3.1 and 3.2) affect the excess free energies of adsorbed intermediates and transition states (i.e., G_A^{\ddagger} , G^{\ddagger}). Second, changes to the solvent composition within multicomponent solvent systems (Section 3.3) affect the free energies of adsorbed complexes and liquid phase reactants (G_A^{\ddagger}). Third, these concepts extend to heterogeneous catalysts besides zeolites (Section 3.4), including metal oxides, metal surfaces, and metal-organic frameworks (MOF). Fourth, these principles also prove useful to understand the solvation effects on the stability of adsorbates and adsorption free energies (ΔG_b , Eq. 7), which determines uptakes and selectivities for adsorption processes (Section 3.5). Finally, interactions between ionic species and solvents affect electrocatalytic, heterogeneous, and homogeneous reactions (Section 3.6) through changes in free energies of reactive species, ionic additives, and catalysts.

3.1 Effects of Zeolite Polarity on Solvation

Zeolites are microporous, silicate materials that can accommodate metal heteroatoms (e.g., Ti^{4+} , Sn^{4+} , Al^{3+}) within the crystalline framework, which provide chemically distinct sites with useful catalytic and adsorptive properties. Catalytic reactions within zeolite pores depend sensitively on solvent choice because the structure of solvation shells for reactive species must undergo significant changes as reactants enter pores, bind to active sites, and molecularly rearrange as a reaction progresses. The number of active sites and defect hydroxyl (-OH)

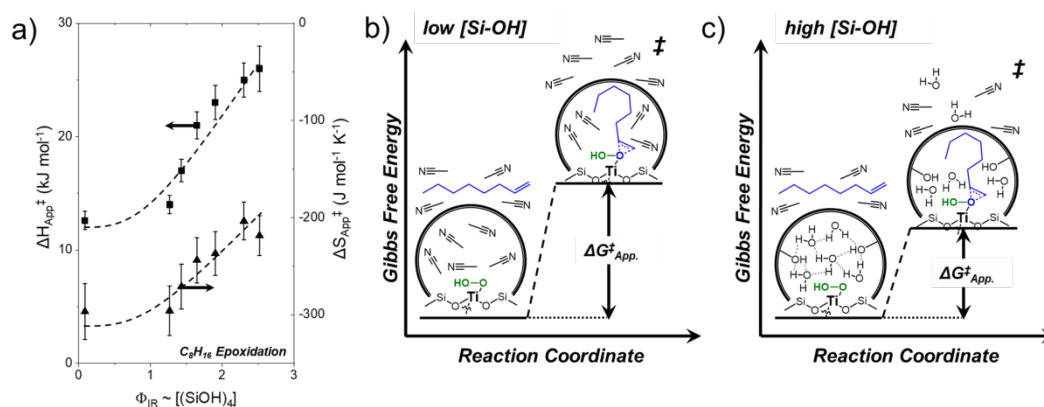


Figure 2. a) Entropies and enthalpies of activation for the epoxidation of 1-octene with H_2O_2 in aqueous acetonitrile solvent as functions of a semi-quantitative measure of silanol group density within Ti-BEA zeolites. Disruption of water network when transition state forms in hydrophilic pores leads to entropic gains (increasing $\Delta S_{App}^{\ddagger}$). b) Schematic free energy diagrams for transition state formation in hydrophobic pores without silanol defects (Si-OH) to stabilize water and c) hydrophilic Ti-BEA pores that stabilizes water networks. Adapted with permission from Ref. 46 and 56. Copyright 2019 American Chemical Society.

functions lead to notable behavioral changes of molecules within these pores, even when all other aspects of the zeolite structure remain fixed. Defect groups and their interactions with solvent molecules also influence the composition of the condensed phase within pores and the structural arrangements those solvent molecules adopt to minimize free energy. These structures, in turn, influence the stability of reactive species found among the solvent molecules within these pores through molecular interactions (*vide infra*).

The kinetics of alkene epoxidations within Lewis acid zeolite catalysts in organic solvents depend on the solvent structure and pore polarity. Several studies demonstrated that hydrophilic zeolites lead to greater epoxidation rates.⁴⁶⁻⁵⁰ Hydrophilic zeolite pores adsorb greater quantities of water than hydrophobic zeolites because silanol defects (Si-OH) stabilize hydrogen-bonded networks of water molecules within pores, leading to increasingly exothermic enthalpies for water adsorption.^{46, 51-52} Grosso-Giordano et al. found that cyclohexene epoxidation rates with tert-butyl hydroperoxide are 5 times greater over microporous titanium-incorporated zeolites than over mesoporous or nonporous materials.⁵³⁻⁵⁴ They proposed that Si-OH groups within confined micropores interact with peroxide intermediates bound to neighboring titanium sites.⁵³⁻⁵⁴ Silanol moieties hydrogen bond with the distal oxygen of the adsorbed peroxide and, in doing so, lower the energetic barrier for oxygen transfer to the cyclohexene reactant. The He group suggested that Ti-O-Si bonds cleave to form Ti-OH and Si-OH pore functions at Ti(OSi)₃OH sites by treating Ti-MFI zeolite with ethylamine⁴⁸ or increasing nitric acid treatment time for Ti-MWW zeolite.⁴⁹ They attributed increases in 1-hexene, propylene, and cyclopentene epoxidation rates with aqueous hydrogen peroxide (H₂O₂) to a higher density of the strong Lewis acid Ti(OSi)₃OH sites.⁴⁸⁻⁴⁹ Wang et al. showed that treating Ti-MFI with dimethyl dimethoxy silane (DDS) increases 1-hexene epoxidation rates with aqueous H₂O₂.⁵⁵ The authors suggested that the DDS treatment leads to the formation of framework -OH groups but credited the increased rates to an increased H₂O₂ uptake within the pores of the hydrophilic zeolite.⁵⁵ These studies suggest that a greater density of -OH functions (either Ti-OH or Si-OH groups) leads to greater epoxidation rates in Ti-incorporated zeolites.

Our group found that turnover rates for 1-octene epoxidation with aqueous H₂O₂ over Ti-BEA zeolites in acetonitrile solvent increase by a factor of 100 as the number of Si-OH defects increase within the BEA framework.⁴⁶ H₂O₂ decomposition rates do not vary with Si-OH density, causing Ti-BEA zeolites with greater numbers of Si-OH defects to give greater selectivities as well.⁴⁶ We attributed these differences to increased proximities between active sites and water oligomers, which couple the formation of transition states with the disruption of hydrogen bonded water clusters (Fig. 2a).⁴⁶ Fig. 2b and 2c depict the molecular processes responsible for the differences in ΔH_{app}^\ddagger and ΔS_{app}^\ddagger values in hydrophobic and hydrophilic pores, respectively. The formation of the epoxidation transition state from 1-octene and the H₂O₂-derived Ti-OOH complex (the MARI at these conditions) disrupts the solvent structure within the pore. Within the hydrophobic pore environment (Fig. 2b), the formation of the transition state involves displacement and rearrangement of weakly interacting acetonitrile molecules. However, the hydrophilic pore stabilizes hydrogen bonded water oligomers (Fig. 2c), the disruption of which incurs an enthalpic cost but yields more significant entropic gains that lower G_{A^\ddagger} and increase epoxidation rates.^{46-47, 56} The reorganization of solvent water molecules does not affect G_{A^\ddagger} at these conditions,⁴⁶ which leads to a decrease in ΔG_{app}^\ddagger as shown in Eq. 10. Complementary isothermal titration calorimetry (ITC) measurements show that the free energy of 1,2-epoxyoctane adsorption ($\Delta G_{ads,epox}$) correlates linearly with ΔG_{app}^\ddagger .⁵⁶ Epoxide adsorption requires similar solvent reorganization as the formation of the epoxidation transition state; therefore, the correlation between $\Delta G_{ads,epox}$ and ΔG_{app}^\ddagger provides further evidence that solvent structure alters G_{A^\ddagger} .⁵⁶ The effect of solvent molecules on G_{A^\ddagger} agrees with rate increases correlated with greater numbers of intraporous -OH groups in the studies mentioned earlier in this section.^{48-49, 55} In short, water networks provide entropic stabilization when disrupted by the formation of epoxidation transition states.

Hydrophobic Lewis acid zeolites give greater turnover rates for aqueous-phase glucose isomerization than their hydrophilic analogs due to similar solvent excess interactions.^{52, 57-59} For example, Cordon et al. showed that isomerization turnover rates increase by a factor of 5-10 from hydrophilic (Ti-BEA-OH) to hydrophobic (Ti-BEA-F) zeolite.⁵⁹ These increases in rates occur

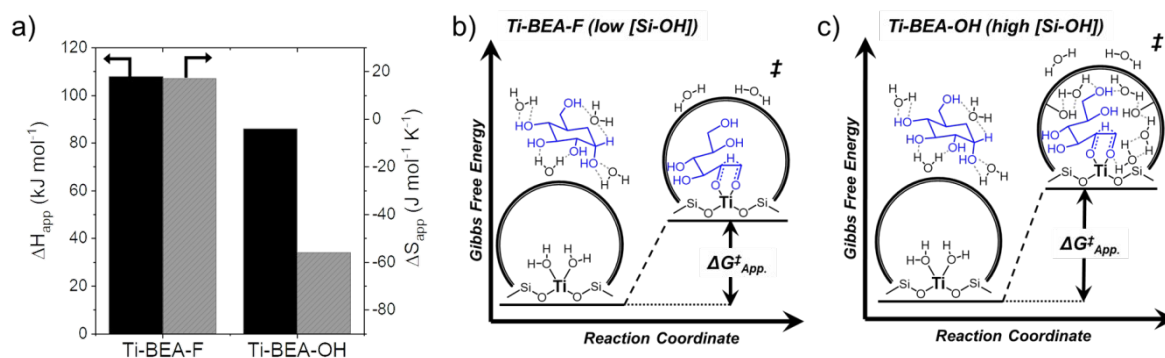


Figure 3. a) Enthalpies and entropies of activation for glucose isomerization in water within hydrophobic and hydrophilic Ti-BEA. Hydrogen bonding between water network and glucose transition state forms in hydrophilic pores leads to entropic losses (decreasing ΔS_{App}^\ddagger). b) Schematic free energy diagrams for transition state with hydrophobic Ti-BEA and c) hydrophilic Ti-BEA. Figure made to illustrate concepts in Ref. 59.

for kinetic regimes, in which rates exhibit a first-order dependence on glucose concentration (two adsorbed water molecules as the MARI) and a zero-order dependence on glucose concentration (bound glucose intermediate as the MARI).⁵⁹ This similarity shows that competitive adsorption effects between water and glucose do not depend on pore polarity and rate differences result from a lower G^{\ddagger} in Ti-BEA-F. Fig. 3a shows that the water network in Ti-BEA-OH leads to a slight enthalpic stabilization relative to Ti-BEA-F but a more significant entropic destabilization that increases G^{\ddagger} , thus increasing γ_{\ddagger} and lowering rates (Eq. 11). The absence of the condensed water phase in Ti-BEA-F pores leads to entropic stabilization of the isomerization transition state compared to Ti-BEA-OH, as illustrated in Fig. 3b and 3c for the regime with adsorbed waters as the MARI. Nevertheless, Cordon et al. discovered in a later study that introducing a slight degree of hydrophilicity to Sn-BEA-F by immersion in hot liquid water improves glucose isomerization turnover rates by about a factor of 2 over untreated Sn-BEA-F.⁶⁰ They attributed the increase in rates to the formation of low densities of Si-OH groups, which stabilize small clusters of water near framework Sn sites.⁶⁰ These water clusters enthalpically stabilize the transition state without the entropy decrease caused by the extended water networks within highly hydrophilic pores. Separately, other studies found that first-order rate constants⁶¹ and conversions⁶² for glucose isomerization over hydrophobic zeolites are greater in liquid methanol than in water. Christianson et al. used density functional theory (DFT) and molecular mechanics to analyze glucose isomerization in methanol and water over Sn-BEA zeolites.⁶³ They attributed greater glucose conversions in methanol to the partial solvation of glucose by methanol molecules within Sn-BEA-F pores and proposed that this lowers the energetic penalty for desolvating glucose during adsorption to the Sn active site.⁶³ Methanol forms a condensed phase in the pores of both hydrophobic and hydrophilic Lewis acid zeolites,^{52, 63-64} while water only does so in hydrophilic pores.⁵² Consequently, glucose loses a large fraction of the solvating water molecules when it adsorbs into a hydrophobic pore from a bulk water phase, yet a greater portion of methanol molecules may co-adsorb with glucose in the pore. Therefore, methanol may provide modest stabilization to transition states through hydrogen bonding without significant entropic destabilization. Collectively, critical comparisons of these studies show that hydrogen bonded networks of water molecules in hydrophilic zeolites inhibit glucose isomerization.^{52, 57-59} Small clusters of protic solvent molecules in hydrophobic zeolites lower

G^{\ddagger} with respect to G_A^{\ddagger} through hydrogen bonding,^{60, 62-63} leading to a decrease in $\Delta G_{app}^{\ddagger}$ (Eq. 8). These observations demonstrate that the greatest glucose isomerization turnover rates result from optimizing the balance between enthalpic stabilization and compensating entropic penalties.

The restructuring of alcohol solvent molecules in hydrophobic and hydrophilic Lewis acid zeolite pores also impacts turnover rates of cyclohexanone transfer hydrogenation.⁶⁵ Di Iorio et al. showed that transfer hydrogenation rates are 10 times greater over Sn-BEA-F than Sn-BEA-OH with 2-butanol as solvent and reductant.⁶⁵ As depicted in Fig. 4, they hypothesized that 2-butanol forms ordered dimeric hydrogen bonding networks in Sn-BEA-F, but oligomeric extended hydrogen bonded networks stabilized by Si-OH groups in Sn-BEA-OH.⁶⁵ They reasoned that the ordered network of 2-butanol molecules in Sn-BEA-F leads to greater solvent displacement when cyclohexanone enters the pore and increases the enthalpy and entropy of adsorption relative to Sn-BEA-OH.⁶⁵ However, $\Delta H_{app}^{\ddagger}$ for the kinetically relevant hydride shift between adsorbed cyclohexanone and 2-butanol decreases in Sn-BEA-F, which they attributed to enthalpic stabilization of the transition state by the ordered 2-butanol structure in the hydrophobic pore.⁶⁵ The structuring of alcohol molecules within zeolite pores may also explain why Ti-MFI-F shows greater $\Delta H_{app}^{\ddagger}$ and $\Delta S_{app}^{\ddagger}$ values than Ti-MFI-OH for 1-octene epoxidation with aqueous H_2O_2 in methanol solvent.⁶⁶ Methanol molecules may form networks with short range ordering within Ti-MFI-F and oligomeric extended structures in Ti-MFI-OH. The disruption of the ordered methanol network in Ti-MFI-F by the 1-octene epoxidation transition state likely leads to greater values of $\Delta H_{app}^{\ddagger}$ and $\Delta S_{app}^{\ddagger}$ than disrupting the oligomeric network in Ti-MFI-OH.⁶⁶ These studies demonstrate that zeolite pore functions affect the structure of alcohol solvent networks, which determines the degree of solvent reorganization required to accommodate the adsorption of reactive species, and by extension, affects G_A^{\ddagger} and G^{\ddagger} .

This section shows that the arrangement of solvent molecules around active sites in a zeolite pore affects the adsorption and stabilization of reactive species, significantly impacting reaction rates. The solvent environment within the zeolite depends on pore polarity and solvent choice. Hydrophobic reactants (e.g., in alkene epoxidation) show enhanced reactivity in hydrophilic pores containing water, while hydrophilic reactants (e.g., in glucose isomerization or cyclohexanone transfer hydrogenation) prefer empty or alcohol-filled hydrophobic pores. The appropriate pairing of transition states with solvents and solvating pore environments provides opportunities to selectively lower G^{\ddagger} and increase reaction rates and selectivities, as seen for alkene epoxidations with H_2O_2 .

3.2 Effect of Zeolite Framework on Solvent and Reactant Structure

The confining environment of a zeolite pore (typically less than 1 nm) forces solvent molecules to adopt different configurations than in the bulk solvent. The confined solvent structures interact with reactants in the pore, affecting G_A^{\ddagger} and G^{\ddagger} and influencing reaction rates (Note: an increase in G^{\ddagger}

a) Sn-BEA-F (low [Si-OH]) b) Sn-BEA-OH (high [Si-OH])



Figure 4. Alcohol solvents (ROH) a) interacting with silanol defects (Si-OH) and forming a) dimeric H-bonding networks in a hydrophobic pore and b) an extended liquid-like H-bonding network in a hydrophilic Sn-BEA pore. Made to illustrate concepts in Ref. 65.

represents a change where G^\ddagger becomes more positive; i.e., the species is destabilized). Myriad zeolite frameworks provide a vast array of pore topologies with distinct diameters and shapes for pores and voids formed at their intersections. The large range of variations in the environments surrounding catalytic active sites gives rise to consequential differences in solvent structure that impact the stability of reactive species even when the zeolite frameworks possess similar numbers of hydrogen bonding Si-OH groups.

Wang et al. demonstrated that water solvates and mobilizes reactive protons in Brønsted acid zeolites that electronically balance framework Al^{3+} atoms.⁶⁷ These interactions form protonated water clusters within the pores and can delocalize protons relative to their equilibrium positions within dehydrated conditions.⁶⁸ Bates et al. studied ethanol dehydration over Brønsted acid zeolites with a range of mean pore diameters, including H-Al-CHA (0.38 nm pores), -MFI (0.55 nm), -BEA (0.65 nm), and -FAU (1.3 nm).⁶⁹ They collected transmission infrared spectra while flowing water and ethanol vapor to qualitatively examine hydrogen bonding among water and ethanol molecules within the pores, and compared these spectra to results from *ab initio* simulations to confirm the formation of protonated clusters of ethanol and water.⁶⁹ They demonstrated that the zeolite pore size affects reactivity by stabilizing the ethanol-water cluster MARI and bimolecular ethanol dehydration transition state to different extents. Van der Waals interactions with the pore walls stabilize the larger $[C_2H_5O(H)---(C_2H_5)^+---OH_2(H_2O)_n]$ transition states more significantly than the smaller $(C_2H_5OH)(H_3O^+)(H_2O)_n$ MARI, lowering G^{\ddagger} compared to $G_{A^*}^\ddagger$ and thus lowering ΔG_{app}^\ddagger (Eq. 10).⁶⁹ The resulting increase in apparent rate constants for smaller pore zeolites couples with a greater tendency for water to aggregate near active sites and inhibit rates. The authors attributed the inhibition to greater barriers to reorganize water networks in response to transition state formation in the most tightly confined pores.⁶⁹ Therefore, varying the zeolite pore size leads to competing effects of dispersive stabilization and solvent competition for active sites that alter $G_{A^*}^\ddagger$ and G^{\ddagger} .

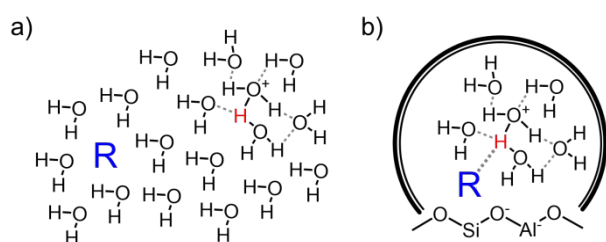


Figure 5. a) Greater numbers of water molecules present per reactant (R) in a Brønsted acid catalyzed homogeneous reaction leads to an increased mean distance between the reactant and catalytic hydronium ion compared to b) a zeolite catalyzed reaction. Figure made to illustrate concepts in Ref. 70–73.

Recent work from the Lercher group shows that zeolite confinement and proton solvation affect reactant adsorption and several aqueous-phase Brønsted acid catalyzed reactions within aluminosilicate zeolites. For aqueous phase alcohol dehydration, rates increase by a factor of 15 to 1000 when confined water molecules solvate protons and transition states in comparison to the homogeneous reaction.^{70–73} For example, H-BEA gives rates of

cyclohexanol dehydration 15 times greater than those for homogeneous H_3PO_4 when normalized by the number of catalytic protons.⁷⁰ Complementary adsorption measurements of cyclohexanol and water uptake indicate that H-BEA contains about 5 cyclohexanol and 20 water molecules per unit cell. In comparison, the liquid phase possesses only 1 cyclohexanol molecule among 180 water molecules, which demonstrates preferential uptake of the reactant within the zeolite.⁷⁰ Fig. 5 illustrates that a larger fraction of hydronium ion ($H^+(H_2O)_n$) clusters associate with cyclohexanol molecules in H-BEA, which increases rates with respect to the homogeneously catalyzed reaction. Cyclohexanol shows similar values of ΔH_{app}^\ddagger for dehydration in H_3PO_4 and over H-BEA but higher values of ΔS_{app}^\ddagger over H-BEA. The authors reasoned that the lower entropy of the intermediates in zeolite pores leads to a smaller entropy loss when forming the dehydration transition state.⁷⁰ Separately, Shi et al. examined the effect of pore size on aqueous phase cyclohexanol dehydration and found that H-MFI gives greater rates than larger pore H-BEA and H-FAU zeolites.⁷¹ H-MFI binds cyclohexanol most exothermically and shows the lowest dehydration ΔH_{app}^\ddagger compared to H-BEA and H-FAU, which they attributed to stabilization of the adsorbed intermediate and transition state by van der Waals interactions with the pore walls.⁷¹ Alternatively, these rate differences may result from interactions with the $H^+(H_2O)_n$ cluster in the tighter confines of H-MFI destabilizing adsorbed cyclohexanol (a relatively hydrophobic molecule) more significantly than in larger pores, which increases $G_{A^*}^\ddagger$ and decreases ΔG_{app}^\ddagger (Eq. 10). Eckstein et al.⁷⁴ and Pfriem et al.⁷⁵ showed that H-MFI zeolites with greater concentrations of Brønsted acid ($H^+(H_2O)_n$) sites (i.e., more hydrophilic) lead to increased activity of adsorbed cyclohexanol (γ_{A^*}). The $H^+(H_2O)_n$ cluster also stabilizes the positively charged transition state for cyclohexanol dehydration, leading to an initial decrease in ΔG_{app}^\ddagger as $H^+(H_2O)_n$ concentrations increase.⁷⁵ Rates eventually decrease at higher $H^+(H_2O)_n$ concentrations, which results from competitive adsorption effects (discussed in Section 5.2).

The Lercher group also demonstrated that solvent and reactant identity impact Brønsted acid catalyzed reactions and described similar intermolecular phenomena that underpin these effects. For example, Shetty et al. showed that dehydration rates of secondary alcohols are greater in H-MFI than H-BEA,⁷² which they attribute to van der Waals stabilization lowering ΔH_{app}^\ddagger for alcohol dehydration in the smaller MFI pores. Tertiary alcohols, however, show lower values of ΔH_{app}^\ddagger and greater dehydration rates in the larger pore H-BEA than H-MFI.⁷² The authors found that H-BEA shows a greater ratio of alcohol reactant to $H^+(H_2O)_n$ site than H-MFI, which they postulated to signify that surrounding reactant alcohol molecules solvate and stabilize the transition state through dispersive interactions more effectively in H-BEA than H-MFI.⁷² A similar study by Chen et al. on cyclohexanol dehydration using H-MFI, -BEA, and -FAU shows the greatest dehydration rates on H-FAU within a nonpolar decalin solvent.⁷⁶ They hypothesized that intraporous decalin and cyclohexanol molecules lower ΔH_{app}^\ddagger in H-FAU through dispersive interactions, while these interactions play less of a role in H-MFI because the

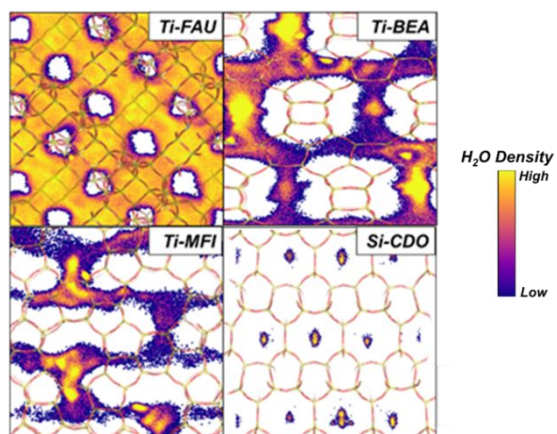


Figure 6. Two-dimensional heat maps of the position of H₂O molecules within hydrophilic zeolites from MD simulations. Adapted from Ref. 47.

smaller pores impede adsorption of the large solvent and reactant molecules.⁷⁶ Chen et al. also found that each zeolite showed greater cyclohexanol dehydration rates in decalin than water solvent,⁷⁶ as also observed for phenol alkylation in H-BEA.⁷⁷ These trends were taken as evidence that catalytically active protons remain bound to the zeolite framework in decalin, which lowers ΔG_{app}^\ddagger to transfer protons to the reactant in comparison to proton transfer from delocalized hydronium ion clusters formed with water.⁷⁶⁻⁷⁷ These water-solvated protons possess lower G_A^\ddagger than framework protons, which decreases rates per Brønsted acid site by decreasing values of γ_A (i.e., activity of the catalytic proton) (Eq. 11). Coupling the works here with the studies discussed in the previous paragraph shows that the pore size of Brønsted acid zeolites determines how solvent and reactant molecules organize and interact with transition states in the pore, leading to changes in G_A^\ddagger and G^\ddagger .

Our group recently showed that framework topology and polarity impact Lewis-acid catalyzed alkene epoxidation reactions in acetonitrile solvent with aqueous hydrogen peroxide.^{15, 47, 78-79} Specifically, Fig. 6 illustrates that the topology and polarity of the zeolite pores determine the concentration and structuring of water molecules: water forms bulk-like three-dimensional hydrogen bonded structures in large pore Ti-FAU but one-dimensional chains and oligomers in smaller pore zeolites, such as Ti-BEA, Ti-MFI, and siliceous CDO.⁴⁷ *In situ* vibrational spectroscopy and both classical and *ab initio* molecular dynamics (MD) simulations show that the average

number of hydrogen bonds per water molecule ($\langle N_{HB} \rangle$) decreases as the mean void diameter and Si-OH density decrease. These decreases in $\langle N_{HB} \rangle$ lead to greater entropy gains upon the disruption of the water structures near Ti active sites.⁴⁷ The reorganization of these water structures to accommodate the formation of epoxidation transition states likely leads to large entropic gains that offset the enthalpic penalty of breaking these hydrogen bonds (*vide supra*). More specifically, the correlation of ΔH_{app}^\ddagger and ΔS_{app}^\ddagger values for epoxidation reactions depends directly upon the water structures present in the pore. These interpretations are supported by a strong correlation between the temperature dependence of populations of hydrogen bonded water molecules within pores (assessed by infrared spectra) and measured activation parameters. Together, these measurements show that smaller pore zeolites give the greatest entropic gain per enthalpic cost of hydrogen bond disruption because the highly correlated motion of the H₂O molecules significantly decreases the entropy of the confined H₂O structures prior to reorganization during catalysis,⁴⁷ which gives greater decreases in G^{\ddagger} in comparison to G_A^\ddagger that lower ΔG_{app}^\ddagger (Eq. 10). This enthalpy-entropy compensation relationship also explains why the difference in epoxidation rates between hydrophobic and hydrophilic zeolites is greatest for Ti-MFI (0.55 nm pores) and smallest for Ti-FAU (1.3 nm pores). While demonstrated here for epoxidation reactions, these concepts should broadly apply to other reactions catalyzed within microporous materials containing hydrogen bonded solvents (e.g., other zeolites topologies and compositions but also microporous metal oxides and organic frameworks).

Collectively, this section shows that confinement requires solvent molecules to adapt configurations that affect the solvation and stability of active sites and reactive species for Brønsted and Lewis-acid catalyzed reactions. Altering the zeolite pore size can affect G_A^\ddagger and G^{\ddagger} to different extents, which leads to changes in catalytic turnover rates. Combining the findings from this section with those from Section 3.1 shows that controlling the identity of zeolites, solvents, and reactants can alter the values of G_A^\ddagger and G^{\ddagger} and strongly impact liquid phase catalytic processes.

3.3 Solvation Effects in Multicomponent Solvent Systems

Sections 3.1 and 3.2 discussed studies that used a single solvent or one solvent in a large excess of another (i.e., alkene epoxidations with organic solvent and less than 0.01 mole

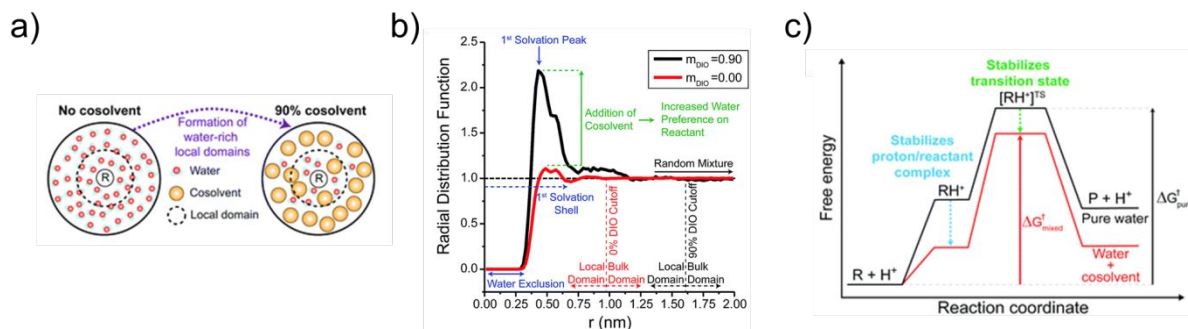


Figure 7. (a) The water content in the local domain increases compared to the bulk when introducing a high content of organic co-solvent, (b) as shown by radial distribution function simulations. (c) The increased water content stabilizes alcohol dehydration transition states. Adapted from Ref. 83 with permission from the Royal Society of Chemistry.

fraction water). This section describes multi-component solvent mixtures, which we define as mixtures containing at least two solvent components with mole fractions of each greater than 0.01. In these mixtures, solvent domains or mixed hydrogen bonded solvent structures form and affect the stability of reactive species for catalytic reactions. For homogeneously acid catalyzed alcohol dehydration reactions, a two-component solvent mixture can partition such that the bulk domain (i.e., far from the alcohol reactant) becomes enriched in one solvent molecule and the domain near the alcohol reactant (i.e., within a length scale < 2 nm) possesses a different composition. The presence of these distinct solvent domains resembles the differences between solvent composition and structure of the bulk fluid and intrapore domains within zeolites (Sections 3.1 and 3.2), albeit without also imposing the confining effects of the zeolite on the solvent structure. This analogy suggests that mixing an organic solvent with water may impact zeolite catalyzed reactions by altering the differences between the solvent environment in the bulk solution and the zeolite pore. In both homogeneous and zeolite catalyst systems, the formation of solvent mixtures can affect the stability of reactants and transition states in ways that change rates significantly.

Turnover rates of homogeneous acid catalyzed alcohol dehydration increase by orders of magnitude upon changing the solvent from water to mixtures containing water and gamma-valerolactone (GVL) co-solvent (>70 % by mass).⁸⁰⁻⁸¹ In the aqueous-organic mixtures, MD simulations show that the bulk domain is enriched in GVL and the local domain around the hydrophilic alcohol reactant is enriched in water.⁸¹⁻⁸³ The reactive proton preferentially resides in the hydrophilic local domain over the bulk GVL phase, increasing the association between the proton and alcohol reactant. As illustrated in Fig. 7, Walker et al. showed that this local water domain stabilizes the protonated alcohol reactant complex while also stabilizing the positively charged transition state that forms, thus lowering G^{\ddagger} .⁸³ Rates are lower in pure water because water solvates the proton in the bulk liquid phase, stabilizing the reactants relative to the transition state and increasing values of $\Delta G_{app}^{\ddagger}$ (Eq. 8).

When water mixes with a more basic organic co-solvent (e.g., dimethyl sulfoxide (DMSO)), the co-solvent may solvate polar reactants more effectively than water. Through MD simulations, Chew et al. found that hydronium ions show lower G^{\ddagger} in DMSO than water.⁸⁴ Their simulations also showed that 1,2-propanediol preferentially interacts with DMSO rather than water,⁸⁴ which suggests that DMSO should concentrate in the local domain surrounding alcohol dehydration transitions states during homogeneous reactions in DMSO-water mixtures. In further work, Chew et al. showed that the primary product of 1,2-propanediol dehydration switches from propanal in pure water to acetone in DMSO-water mixtures.⁸⁵ They attributed the change to the enrichment of both water and DMSO molecules around the hydroxyl groups on 1,2-propanediol that facilitate a distinct reaction pathway (a semipinacol rearrangement) that eliminates the terminal hydroxyl group before yielding acetone.⁸⁵ Mixing DMSO with water decreases G^{\ddagger} of reactive species for acetone

formation compared to propanal formation, making the acetone pathway more favorable.

Adding tetrahydrofuran (THF) to water increases rates for sulfuric acid catalyzed cellulose hydrolysis⁸⁶ and metal halide catalyzed sugar dehydration⁸⁷ relative to pure water, while also enhancing the solubilization of biomass such as cellulose⁸⁶ and corn stover.⁸⁷ MD simulations by Mostofian et al. revealed that THF and water phase separate to hydrophobic and hydrophilic surfaces of cellulose fibers, respectively.⁸⁶ The hydrogen bond lifetime between water molecules and the hydrophilic glycosidic linkages of cellulose increases in THF-water mixtures in comparison to pure water.⁸⁶ This suggests that water molecules stabilize the transition state for cellulose hydrolysis more significantly in the THF-water mixture than in pure water, which decreases G^{\ddagger} and leads to an enhanced rate of cellulose hydrolysis. The homogeneous studies described here show that mixing water with organic co-solvents affects reaction rates by altering values of G_A^{\ddagger} and G^{\ddagger} to different extents and thereby changing $\Delta G_{app}^{\ddagger}$.

The compositions of aqueous organic solvent mixtures also dictate the solvent environment both in bulk solution and in the pores of zeolites or other solid catalysts, which leads to changes in the stability of reactive species in the fluid phase (G_A^{\ddagger}) but also within the pores (G_A^{\ddagger} , G^{\ddagger}). For example, Mellmer et al. showed that xylose dehydration rates over H-BEA zeolite are 40 times greater in an aqueous solution containing 90 wt% GVL than those measured in pure water.⁸⁰ They attributed the changes to the increased solvation of the zeolite proton in neat water that lowers G_A^{\ddagger} with respect to G^{\ddagger} and increases $\Delta G_{app}^{\ddagger}$ (Eq. 8) relative to aqueous GVL.⁸⁰ Separately, Mellmer et al. showed that the levulinic acid yield from furfuryl acid hydrolysis over H-MFI zeolite increases from <10% in pure water to ~70% in a 4:1 THF-water mixture by weight.⁸⁸ They took these differences as evidence for changes in the enrichment of THF in the H-MFI pores for the THF-water mixture, which leads to greater hydrolysis rates than a water-filled pore.⁸⁸ Alternatively, these zeolites possess significant densities of Si-OH functions, as the authors showed by infrared spectroscopy.⁸⁸ In this situation, the pores of the MFI structure likely stabilize networks or clusters of water that solvate reactive species in turn and lower G^{\ddagger} . Concomitantly, the hydrophobic bulk THF phase should destabilize hydrophilic furfuryl alcohol and increase the free energy of the fluid-phase reactant (G_A^{\ddagger}). The effects taken together would decrease values

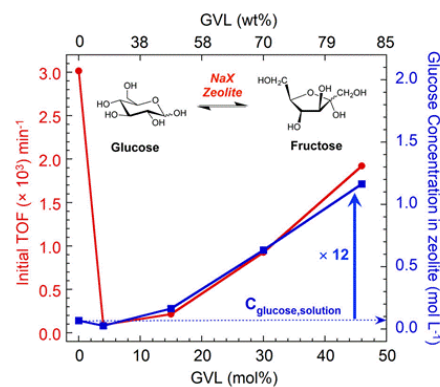


Figure 8. GVL affects catalytic activity for glucose isomerization and glucose uptake into NaX zeolite. Reprinted with permission from Ref. 89. Copyright 2017 American Chemical Society.

of ΔG_{app}^\ddagger (Eq. 8) and would be consistent with the reported differences in rates. Fig. 8 shows results from the work of Qi et al. that reported initial turnover rates for glucose isomerization over Na-exchanged faujasite zeolites (NaX and NaY) decrease by a factor of 300 with the addition of ~ 4 mol% GVL to water.⁸⁹ The uptake of glucose into the zeolite pore (measured with solid-state NMR) decreases upon adding this small amount of GVL, which they explained as the occlusion of glucose by GVL present in the pores.⁸⁹ Measured excess enthalpies of mixing for GVL and water are slightly exothermic (~ -0.1 kJ mol⁻¹) at GVL mole fractions below 0.1 and endothermic (maximum +0.8 kJ mol⁻¹) at higher mole fractions,⁹⁰ which suggests that water and GVL likely mix in the pore at low GVL concentrations. Qi et al. argue that GVL disrupts water in the pores and limits the ability of water molecules to stabilize reactive species at low GVL concentrations.⁸⁹ This reasoning suggests that GVL increases $G^{e,\ddagger}$ relative to G_A^e , which increases values of ΔG_{app}^\ddagger and leads to the 300-fold decrease in rates compared to pure water. Glucose isomerization rates and glucose uptake in the zeolite pore increase with GVL content, with a 12-times greater uptake observed in a mixed solvent with 46 mol% GVL than in pure water. At higher GVL contents, G_A^e of glucose in the bulk GVL phase should increase with respect to the transition state and lead to a decrease in ΔG_{app}^\ddagger (Eq. 8).

The studies in this section collectively demonstrate that mixing solvents affects the reaction environment and stability of reactive intermediates and transition states for both homogeneous and zeolite catalyzed reactions. The reaction environment in a solvent mixture depends on solvent composition and active site surroundings (i.e., within the zeolite pore or the first- and second-coordination spheres of homogeneous catalysts). Furthermore, tuning the solvent composition of a mixture affects reactive species stability (G_A^e , $G_{A^e}^e$, $G^{e,\ddagger}$), which affects ΔG_{app}^\ddagger and alters rates and selectivities for desired and undesired reaction pathways.

3.4 Solvent Interactions within Mesoporous Materials and over Metal Nanoparticles

Like the zeolite studies discussed so far, solvents also impact the stability of reactive species in reactions with other solid catalysts, such as mesoporous catalysts, metal nanoparticles, and MOF. These catalysts possess pores and voids of greater dimensions than many zeolites and therefore contain condensed phases around active sites that more closely resemble the structure of the bulk solvent. Nevertheless, solvent molecules organize around and solvate reactive species at the active sites of these catalysts, leading to changes in $G^{e,\ddagger}$ that affect reaction rates (Note: a decrease in G^e represents a change where G^e becomes more negative; i.e., the species is stabilized).

Trimethylphenol oxidation in Cu-Al-MCM-41 mesopores (2.4-2.6 nm diameter) shows greater yields and selectivities in benzaldehyde solvent (69%, 79%) than acetonitrile (47%, 73%), acetaldehyde (1%, 2%), or ethanol (0%, 0%).⁹¹ Yields and selectivities also increase when using bulky tert-butyl hydroperoxide (TBHP) (88%, 89%) as the oxidant instead of hydrogen peroxide (69%, 79%).⁹¹ The transition state for trimethylphenol oxidation may be stabilized by dispersive

interactions with the bulky benzaldehyde solvent molecules and the tert-butyl group in TBHP, leading to a decrease in $G^{e,\ddagger}$. The large mesopores in MCM-41 presumably afford freedom of motion to the transition state, oxidant, and solvent molecules needed to assume favorable configurations that lead to stabilizing dispersive interactions. This proposal agrees with recent work from our group that showed mesoporous Ti-SBA-15 allows for favorable interactions between adsorbed 1-octene and bulky TBHP or cumene hydroperoxide oxidants as compared to microporous Ti-BEA zeolite.⁷⁹ We found that the transition state for 1-octene epoxidation could adopt more configurations in the Ti-SBA-15 mesopores, which lowers its free energy relative to Ti-BEA.⁷⁹ These studies show that the use of mesoporous catalysts promotes dispersive interactions between bulky transition states and solvent molecules that decrease $G^{e,\ddagger}$ and ΔG_{app}^\ddagger (Eq. 8 and 10).

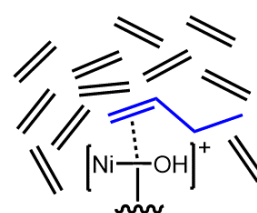


Figure 9. The desorption transition state for the product of ethene dimerization over Ni-Al-MCM-41 is stabilized through dispersive solvating interactions with surrounding condensed phase ethene molecules. Made to illustrate concepts in Ref. 92-93.

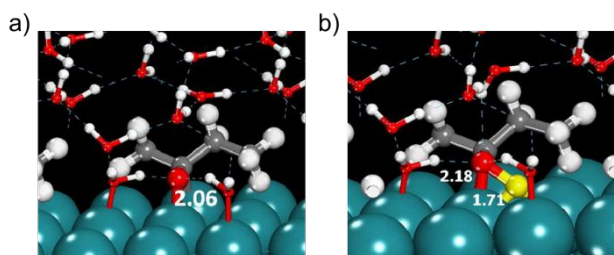


Figure 10. DFT calculated binding configurations for a) molecularly adsorbed 2-butanone and b) the transition state of 2-butanone hydrogenation over Ru(001) in the aqueous phase. The hydrogen atom involved in hydrogenation is shown in yellow. Adapted from Ref. 100, with permission from Elsevier.

The presence of a condensed non-polar phase (e.g., liquid alkene/alkane) in Ni-Al-MCM-41 mesopores (1.0-2.2 nm diameter) enhances the dimerization of ethylene to butenes.⁹²⁻⁹³ Dimerization rates increase by factors of 2-3 and selectivities increase by factors of 2-6 when the reaction temperature decreases from 448 to 248 K, which the authors attributed to condensation of the alkene reactants within the mesopores.⁹²⁻⁹³ Fig. 9 shows that the butene product desorbs through a late transition state that possesses a lower G^{\ddagger} when interacting with a condensed alkene phase in the pore. The condensed phase also prevents deactivation of the catalyst by increasing selectivity to dimer products and limiting the formation of oligomers that bind strongly and block Ni sites. Similar promotion of dimerization and reduction of deactivation rates also occur when inert alkanes are co-fed and condensed within pores, which suggests that these benefits stem from non-specific interactions between the nonpolar condensed phase and reactive complexes.⁹² The critical role of these non-specific interactions agrees with results from Madrahimov et al. in their examination of ethylene dimerization over Ni sites contained within a MOF (NU-1000-bpy-NiCl₂).⁹⁴ They found that carrying out the reaction in liquid n-heptane increases rates and selectivities to the dimer product compared to the gas phase reaction. Farrusseng and co-workers achieved similarly high selectivities to ethylene dimerization products in n-heptane over the MOF Ni@(Fe)MIL-101.⁹⁵ The condensed phase likely leads to similar effects in the MOF as observed in detailed analysis within Ni-Al-MCM-41 mesopores, enhancing the desorption of dimer products by solvating the desorption transition state to lower G^{\ddagger} relative to that of oligomerization product transition states.

Introducing a condensed solvent phase also affects $\Delta H_{app}^{\ddagger}$ for cyclohexene epoxidation over mesoporous transition metal silicate catalysts (6 nm pore diameter). Ahn et al. showed that Ti-SiO₂ and Nb-SiO₂ give similar values for $\Delta H_{app}^{\ddagger}$ in the vapor phase with anhydrous H₂O₂, but Ti-SiO₂ gives an $\Delta H_{app}^{\ddagger}$ value 29 kJ mol⁻¹ lower than Nb-SiO₂ in liquid acetonitrile solvent with aqueous H₂O₂.⁹⁶ They proposed a transition state structure that includes a coordinated solvent molecule (water or acetonitrile) over Ti-SiO₂,⁹⁷⁻⁹⁸ which may not occur over Nb-SiO₂ due to an additional Nb-OH ligand that hinders solvent coordination. The authors attributed the lower barrier over Ti-SiO₂ to the solvent providing low barrier pathways to shuttle protons during oxygen transfer and stabilize the associated transition state.⁹⁶ Alternatively, these results appear consistent with solvent molecules (either water or

acetonitrile) acting to stabilize the transition state through dispersive interactions or by the formation of hydrogen bonds with the peroxide moiety, which would decrease G^{\ddagger} in comparison to $G_{A^{\ddagger}}^{\ddagger}$, thus decreasing $\Delta G_{app}^{\ddagger}$ (Eq. 10).

The presence of hydrogen bonding solvents impacts the hydrogenation of carbonyl groups within molecules like ketones. Wan et al. found that rates for hydrogenation of 2-butanone over Ru/C are much greater in protic solvents than aprotic solvents, with the greatest rates in water.⁹⁹ They found that protic solvents hydrogen bond with 2-butanone and surmised that this decreases $\Delta H_{app}^{\ddagger}$ for hydrogenation. They found that rates correlate to the Kamlet-Taft parameter α (i.e., the hydrogen bond donor ability)²³ of the solvent and suggested stronger hydrogen bond donors interact favorably with the C=O bond in the hydrogenation transition state, which would decrease G^{\ddagger} .⁹⁹ Akpa et al. examined the same reaction over Ru/SiO₂ and found that rates in water are 7 and 33 times greater than in 2-propanol or methanol solvents, respectively.¹⁰⁰ They also attributed the greater rates in water to a decrease in $\Delta H_{app}^{\ddagger}$ from hydrogen bonding between water and the O-H bond forming in the hydrogenation transition state.¹⁰⁰ We concur that protic solvents stabilize the surface-bound transition state for hydrogenation but emphasize that they must do so more significantly than the extent by which these interactions stabilize the adsorbed 2-butanone intermediate, such that G^{\ddagger} decreases to a greater degree than $G_{A^{\ddagger}}^{\ddagger}$ and ultimately reduces $\Delta G_{app}^{\ddagger}$ (Eq. 10). As suggested by Fig. 10, DFT calculations show that the nascent O-H bond makes the transition state more sensitive to the presence of water than adsorbed 2-butanone, which presents the O atom of the ketone function but does not possess apparent hydrogen bond donors. Additionally, the greater rates in 2-propanol than in methanol suggest that dispersive interactions between 2-propanol molecules and the 2-butanone hydrogenation transition state may decrease G^{\ddagger} in 2-propanol compared to methanol. Separately, microkinetic modeling studies by Heyden, Bond and co-workers examined similar effects for hydrodeoxygenation (HDO) reactions. HDO reactions of propionic acid over Ni¹⁰¹ and levulinic acid upon Ru¹⁰² proceed at greater rates in aqueous solutions than in the vapor phase. They attributed these increases in rate to water molecules lowering G^{\ddagger} for HDO pathways through hydrogen bonding with transition state structures. However, the presence of liquid water leads also to stronger adsorption of reactants to the catalyst surface for HDO of propionic acid over Pt¹⁰³ and Pd¹⁰⁴ and methyl propionate over Pd,¹⁰⁵ which decreases rates relative to the vapor phase. These observations suggest that water decreases $G_{A^{\ddagger}}^{\ddagger}$ with respect to G^{\ddagger} for HDO pathways, thus increasing $\Delta G_{app}^{\ddagger}$ (Eq. 10). Additionally, the fact that water increases rates for propionic acid HDO over Ni¹⁰¹ but decreases rates over Pt¹⁰³ and Pd¹⁰⁴ suggests that the identity of the metal also plays a role in solvent-reactant interactions. The impact of hydrogen bonding solvents on hydrogenation and HDO reactions depends on the active metal identity and the relative stabilizing effects of the solvent on adsorbed intermediates and transition states.

This section demonstrates that solvating interactions affect the stability of reactive species for several classes of solid catalysts beyond zeolites. Solvent molecules organize around

intermediates and transition states at the surface of these catalysts and affect rates, but the magnitudes of these rate differences are generally smaller than those discussed previously for microporous materials (Sections 3.1 and 3.2). The solvent structures in bulk solvent and around the active site are likely more similar upon mesoporous materials, MOF, and metal nanoparticles, which causes excess interactions with solvent molecules to have less significant effects on rates (e.g., commonly less than a 10-fold change). These findings indicate that similar principles to those discussed for microporous materials can guide the selection of appropriate catalyst and solvent combinations for chemical processes over other solid catalysts.

3.5 Effect of Solvent Structure on Adsorption Processes

Solvents selectively stabilize certain solutes in the liquid phase relative to the components adsorbed onto a solid catalyst, altering G^\ddagger values and leading to changes in ΔG_I (Eq. 7). These effects parallel the phenomena described for transition state stabilization in prior sections. The presence and identity of a solvent, therefore, affects liquid phase adsorption and separation

polar solvents (e.g., vacuum) and reacts with pyridine more readily, which agrees with the conclusions from Lercher et al. regarding Brønsted acid catalyzed cyclohexanol dehydration in decalin and water (Section 3.2). Overall, the free energy change for pyridine to adsorb to the active site (ΔG_I) increases in nonpolar solvents because these solvents lower G_{A^\ddagger} of the adsorbed pyridinium intermediate more significantly than fluid-phase pyridine (G_A^\ddagger) (Eq. 7). Ancillary studies on the same materials using temperature-programmed desorption show that pyridine desorption shifts to lower temperatures with increasing solvent polarity, which indicates that more polar solvents lead to weaker binding of pyridine (less negative ΔG_I) and corroborates the prior conclusion.¹⁰⁶

Several recent studies used Monte Carlo simulations to examine the separation of alcohol-water mixtures with purely siliceous hydrophobic MFI¹⁰⁸⁻¹¹⁰ and FER¹¹⁰ zeolites. For mixtures of water with methanol,¹⁰⁸⁻¹⁰⁹ ethanol,¹⁰⁸⁻¹⁰⁹ or 1-butanol,¹¹⁰ alcohols adsorb preferentially at the lowest intrapore concentrations, but the selectivity to adsorb alcohols decreases significantly once pores attain a critical density of alcohol

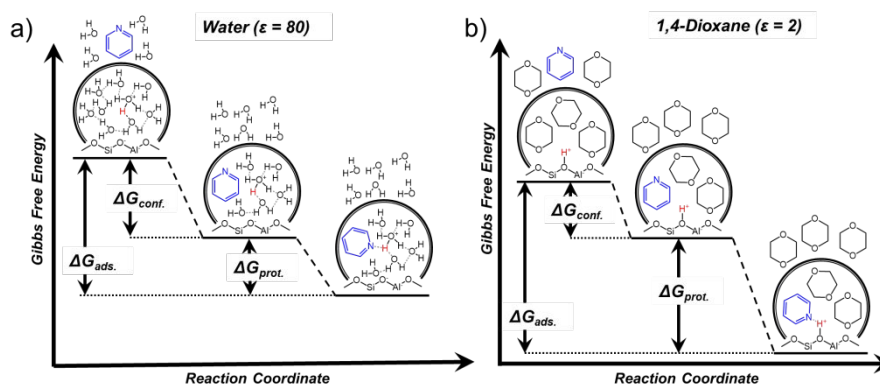


Figure 11. The stabilities of the catalytic proton and liquid phase pyridine in water and 1,4-dioxane (solvents that show a large difference in dielectric constant ϵ) lead to differences in the favorability of pyridine being confined in the H-BEA pores ($\Delta G_{conf.}$) and then being protonated ($\Delta G_{prot.}$). Made to illustrate concepts in Ref. 106-107.

processes onto porous or nonporous solid catalysts.

Gould et al. examined the adsorption and desorption of pyridine into H-BEA pores in distinct solvents (e.g., water, acetonitrile, 1-4 dioxane, n-heptane).¹⁰⁶⁻¹⁰⁷ Fig. 11 shows the differences in adsorption between polar water solvent and less polar 1,4-dioxane solvent. The authors found that the solvent dielectric constant (ϵ) (i.e., a measure of polarity) affects the equilibrium constant for pyridine adsorption to the Brønsted acid sites (K_I), and thus, modifies the free energy for pyridine adsorption ($\Delta G_I = -RT \ln(K_I)$). As the dielectric constant of the solvent increases, the uptake of pyridine into the pores and the confinement equilibrium constant increases, indicating that the free energy change ($\Delta G_{conf.}$) becomes more negative.¹⁰⁷ Pyridine, a relatively nonpolar molecule compared to water, interacts unfavorably with bulk water and shows a greater free energy difference between the bulk and zeolite phases in polar solvents than nonpolar solvents.¹⁰⁷ However, Gould et al. found that the proton transfer equilibrium constant increases, and the protonation free energy change ($\Delta G_{prot.}$) becomes more negative as the solvent polarity decreases. This difference occurs because the catalytic proton possesses a higher free energy within less

molecules. These findings show that the formation of alcohol clusters within hydrophobic zeolites promotes water adsorption by lowering G_{A^\ddagger} of adsorbed water molecules, suggesting that alcohol molecules provide sites for water to hydrogen bond even when such sites are absent from vacant hydrophobic pores. Separately, a study on water mixtures with methanol and ethanol in a number of zeolite topologies (FAU, MFI, DDR, and LTA) revealed that hydrogen bonds between alcohol and water molecules represent a larger fraction of total hydrogen bonding interactions than those between identical molecules.¹¹¹ These findings indicate that water-alcohol interactions predominate over water-water or alcohol-alcohol interactions within these mixtures. Notably, the free energy of mixing water and alcohol molecules within zeolite pores differs from that within the bulk fluid phase for a system equilibrated with a given solvent composition, and this distinction allows for the separation of alcohol-water mixtures. The presence of water-alcohol bonding in these mixtures introduces thermodynamic non-idealities that have consequences for adsorption processes but also for catalysis, as discussed above.

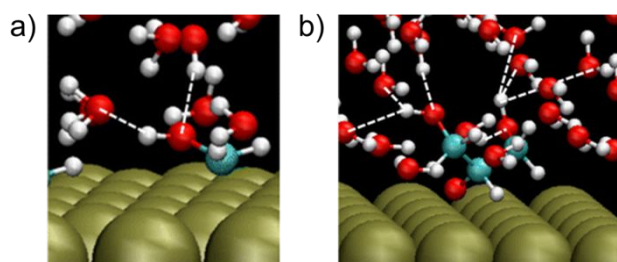


Figure 12. MD simulations showing the hydrogen bonding interactions of water molecules with a) adsorbed CH_2OH and b) adsorbed $\text{C}_3\text{H}_7\text{O}_3$ over a Pt(111) surface. Reprinted with permission from Ref. 118. Copyright 2015 American Chemical Society.

Metal-organic frameworks (MOF) can selectively adsorb compounds from the liquid phase for similar reasons. While these adsorption processes may be driven by covalent or ionic bonding at metal-oxide nodes in many cases, differences in excess free energies also influence these processes. For example, solvent molecules within MOF pores influence the removal of toxic dyes¹¹²⁻¹¹³ from bulk solvent. Haque et al. demonstrated that the adsorption of the large dye molecules methyl orange and methylene blue from water into Fe-MOF-235 led to large increases in entropy that offset corresponding increases in enthalpy.¹¹² The dye molecules disrupt hydrogen bonds among intrapore water molecules as they adsorb, providing entropic gains that decrease $G_{A^{\text{e}}}$ and give more negative ΔG_I values (Eq. 7). As described for zeolites in Section 3.1, the polarity of MOF pores determines the type of structures that solvent molecules form and impacts separation¹¹⁴ and adsorption¹¹⁵⁻¹¹⁶ efficiency. For example, Huang et al. modified -OH defects in the MOF UiO-66 to alter the efficiency of adsorptive oil/water separations.¹¹⁴ They found that the defect dense MOF samples (i.e., more hydrophilic) preferentially reject aliphatic hydrocarbons (e.g., hexane, n-decane, cyclohexane) and give nearly perfect separations for mixtures of hydrocarbons and water.¹¹⁴ The hydrophilic UiO-66 MOF leads to a lower $G_{A^{\text{e}}}$ for water than the alkanes, which causes the MOF to preferentially adsorb water molecules. In another study, Rieth et al. varied the pore size and hydrophilicity of the MOF $\text{Ni}_2\text{Cl}_2\text{BTDD}$ by exchanging Cl^- with other anions.¹¹⁶ The partial pressure of water required to achieve spontaneous pore condensation was lower for Br-modified materials than the Cl-exchanged MOF. The authors demonstrated that introducing bromide contracts the MOF pore diameter, which they proposed to improve the favorability of water uptake by increased confinement that lowers $G_{A^{\text{e}}}$ of adsorbed water.¹¹⁶ This work also showed that water molecules form the lowest average number of hydrogen bonds in the Br-exchanged MOF at low water partial pressures, which may result from the relative hydrophobicity of Br-moieties and concomitant pore constriction that reduce the number of available configurations for water molecules. The lower number of hydrogen bonds in the Br-exchanged MOF allows water molecules to attach to adsorbed waters with unsaturated hydrogen bonding environments. Collectively, these interactions modify the structure of water clusters in the Br-exchanged MOF in manners that increase adsorption of water molecules. Adsorbed water molecules also promote CO_2 adsorption for the MOF 2-ampd- $\text{Mg}_2(\text{dobpdc})$.¹¹⁷ Adsorbed CO_2 molecules bind with framework amine groups and form ammonium carbamate (R-NH-CO_2^-) chains. These carbamates hydrogen bond with water¹¹⁷ and lower $G_{A^{\text{e}}}$ of adsorbed CO_2 , which leads to more negative values of ΔG_I (Eq. 7). These studies show that the structure of solvent molecules within MOF pores impacts the free energies of adsorbates and depends strongly on the chemical moieties present within the pores.

The presence of solvents also affects adsorption onto metal surfaces. For example, Getman and co-workers found that an aqueous phase lowers the enthalpy of hydrophilic adsorbed intermediates on Pt(111) through hydrogen bonding.¹¹⁸⁻¹¹⁹ Fig. 12 shows that hydroxyl groups of an adsorbed glycerol derivative

(C₃H₇O₃^{*}) form a total of 6-7 hydrogen bonds with surrounding water molecules that enthalpically stabilize this intermediate by 125–145 kJ mol⁻¹, while an adsorbed methanol derivative (CH₂OH^{*}) forms approximately two hydrogen bonds that lower its enthalpy by 60 kJ mol⁻¹.¹¹⁸⁻¹¹⁹ These hydrogen bonds also decrease the entropy of the system containing C₃H₇O₃^{*} more significantly than CH₂OH^{*}, however, the enthalpy difference dominates in this case and leads to lower G_{A^\ddagger} for C₃H₇O₃^{*} in comparison to CH₂OH^{*}.¹¹⁹ The enthalpy/entropy compensation of hydrogen bonds between solvent molecules and the adsorbed intermediates determines if the solvent stabilizes or destabilizes the intermediates. Overall, both surface intermediates carry negative G_{A^\ddagger} , such that the presence of water stabilizes these species compared to the vapor phase. Separately, a computational study by Yang et al. found that the uptake of phloroglucinol onto Pt and Pd surfaces decreases by 20-25% in the aqueous phase relative to the vapor phase.¹²⁰ They credited this to hydrogen bonding between the hydroxyl groups in phloroglucinol and water, stabilizing the phloroglucinol in the bulk aqueous phase (lower G_{A^\ddagger}) with respect to adsorbed phloroglucinol (G_{A^\ddagger}), thus lowering ΔG_1 (Eq. 7). The favorable interactions among water molecules and the hydroxyl groups of these surface intermediates agree with chemical intuition, however, the significance of hydrogen bonds extends also to adsorbates that do not present such obvious pairs of hydrogen bond donors and acceptors. Yang et al. demonstrated that H₂ dissociatively adsorbs less strongly on Pt surfaces in the aqueous phase than the gas phase, because the presence of water lowers the enthalpy of adsorption and leads to a greater entropy loss for H₂ adsorption.¹²¹ The authors attributed this to both the displacement of adsorbed water molecules from the surface and the destabilization of the chemisorbed H atoms (H^{*}) by interactions with surrounding water that increases G_{A^\ddagger} . This destabilization reflects the formation of more ordered water structures at the interface with Pt surfaces in the presence of H^{*}, which simultaneously limit the mobility of H^{*}.¹²¹ The solvation free energy of the reactant state (H₂ in water) was determined to be +18 kJ mol⁻¹ at 298 K,¹²¹ which resembles an estimate of +28 kJ mol⁻¹ from prior work.¹²² Combined, these values show that water increases G_{A^\ddagger} of H₂, which accounts for the limited solubilities of H₂ in aqueous solutions. These values indicate that the corresponding increase in G_{A^\ddagger} for H^{*}, together with the free energy to displace water from Pt surfaces, must be greater to explain the less negative value for ΔG_1 to dissociatively adsorb hydrogen in water (Eq. 7). The findings discussed here show that solvent molecules impact the stability of species in the liquid phase (G_{A^\ddagger}) and adsorbed to metal surfaces (G_{A^\ddagger}), which impacts free energies to bind adsorbates and catalytic intermediates (ΔG_1) (Eq. 7).

This section demonstrates that solvent choice affects adsorption and separation processes onto several classes of solid catalysts. The solvent can selectively increase or decrease G_{A^\ddagger} of fluid-phase molecules, affecting how strongly these molecules adsorb onto solid catalysts. The solvent structure within nanometer-scale pores of zeolites and MOF and at nonporous

metal surfaces differs from that in the liquid phase, with variations diminishing as an exponential function of distance from the solid-liquid interface. Consequently, microporous materials exhibit adsorption selectivities that differ significantly from nonporous surfaces that expose similar chemical functions. The local solvent structure influences G_{A^\ddagger} for molecules adsorbing into the pore. Effective combinations of solvent and adsorbates can alter G_{A^\ddagger} and G_{A^\ddagger} to improve the efficiency of adsorption and separation processes.

3.6 Solvation of Ionic Reactants, Additives, and Catalysts

Solvents interact with and affect the activity of ions in solution, as theorized by Brønsted¹²³ and Debye and Hückel²² nearly a century ago. The ions alter the hydrogen bonded networks within protic solvents through the formation of individual solvation shells. Additionally, solvated ionic additives influence reactive species through hydrogen bonds and dipole-dipole interactions. These interactions apply to charged reactants and transition states relevant in many homogeneous²¹ and electrocatalytic reactions.¹²⁴ Solvent molecules may also solvate and stabilize ionic catalytic species that promote homogeneous¹²⁵ and heterogeneous¹²⁶ processes.

Salt additives often dissociate in solvents and selectively stabilize charged reactants and transition states. For example, Enslow and Bell utilized kinetic measurements and ¹³C and ¹H NMR to demonstrate that alkali metal halide additives affect rates of xylose dehydration catalyzed by homogeneous Brønsted acids (e.g., HCl) through direct interactions between the salt ions and reactive intermediates.¹²⁷ The metal cations interact with oxygen atoms in xylose and weaken the C-O bonds that cleave during dehydration, while the halide ions stabilize carbocation intermediates for the reaction. In addition, the ions from the metal halide disrupt stabilizing interactions between water and reactive species, which increases values of G^\ddagger for reactants in comparison to $G^{\ddagger\ddagger}$ and increases rates as a result.¹²⁷ Separately, Mellmer et al. found that adding chloride salts to polar aprotic organic solvents mixed with water (10% by mass) increased rates of fructose dehydration by homogeneous acids by factors of 3 to 10 with respect to the reaction without chloride additives.⁸² MD simulations showed that the local environment around the hydrophilic fructose reactant contains a high concentration of water that solvates Cl⁻ anions, which stabilize the positively charged transition state through electrostatic interactions that lower $G^{\ddagger\ddagger}$ and ΔG_{app}^\ddagger (Eq. 8).

Solvents also form catalytic complexes with active site ions. For example, Choudhary et al. found that Lewis acid metal salts dissociate in water to form hydrated complexes that catalyze homogeneous glucose isomerization.¹²⁵ This process occurs for metal chloride (MCl_x) catalysts including CrCl₃,^{125, 128} AlCl₃,¹²⁹⁻¹³⁰ and SnCl₄.¹³¹ The catalytically active hydrated metal chloride complexes bind a combination of water molecules and hydroxyl (-OH) groups (i.e., [M(H₂O)_x(OH)_x]^{x+}). MD simulations show that the -OH group in the Cr complex ([Cr(H₂O)₅(OH)]²⁺) lowers ΔG_{app}^\ddagger for the glucose ring opening to 125 kJ mol⁻¹ from a barrier of 272 kJ mol⁻¹ in the absence of the -OH group.¹²⁸ Others proposed a mechanism in which the -OH group can facilitate the reaction by abstracting a proton from glucose.^{130, 132} These studies show that

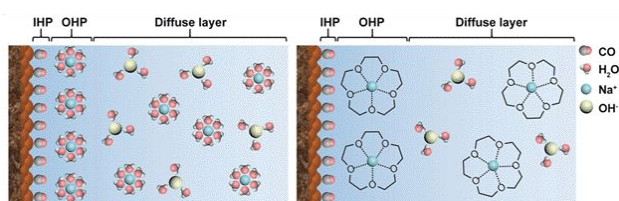


Figure 13. Crown ethers chelate with sodium ions, leading to a decreased concentration of hydrated sodium ions in the outer Helmholtz plane. Reproduced from Ref. 138. Copyright 2019 Wiley-VCH Verlag GmbH & Co. KGaA, Weinheim.

water molecules react with and solvate Lewis acidic metal atoms to form new species that catalyze glucose isomerization. A similar effect occurs for active sites in Cu-exchanged zeolite catalysts. In the selective catalytic reduction (SCR) of nitrogen oxides (NO_x) with ammonia, Paolucci et al. demonstrated that ammonia solvates and mobilizes the Cu ions in $[\text{Cu}^{\text{I}}(\text{NH}_3)_2]$, $[\text{Cu}^{\text{I}}(\text{NH}_3)_4]$, and $[\text{Cu}^{\text{II}}(\text{OH})(\text{NH}_3)_3]$ complexes in Cu-exchanged CHA zeolites.¹³³ Once solvated, the mobile copper ions move between the cages of Cu-CHA zeolite and form Cu site pairs, which activate oxygen for the SCR cycle.¹³⁴ The mobility of these active Cu complexes allows for steady-state interconversion between isolated ($[\text{Cu}^{\text{I}}(\text{NH}_3)_2]$) and paired ($[\text{Cu}^{\text{II}}(\text{NH}_3)_4]$, $[\text{Cu}^{\text{II}}(\text{OH})(\text{NH}_3)_3]$) Cu ions that catalyze the reduction and oxidation SCR cycles, respectively.¹²⁶ Thus, solvation leads to the formation of dynamic Cu active sites that mediate multiple reaction cycles, which would prove difficult for immobile Cu ions tethered to the zeolite framework. These works demonstrate that solvents can form catalytic complexes with and lower G^{\ddagger} of ionic catalyst sites. The solvated homogeneous or heterogeneous catalytic complexes can mediate alternate reaction mechanisms with lower $\Delta G_{\text{app}}^{\ddagger}$ than those observed upon desolvated catalysts.

Interactions between ionic complexes and solvent molecules also affect electrocatalytic reactions at electrode-solvent interfaces. For example, alkali metal cations impact the product distribution of aqueous-phase electrochemical CO_2 reduction (CO_2RR).¹³⁵⁻¹³⁷ Fig. 13 shows that the solvent environment at the electrode-water interface consists of three regions: the inner Helmholtz plane (IHP) that contains water and anions adsorbed to the electrode, the outer Helmholtz plane (OHP) which consists of cations solvated by water, and a diffuse layer containing excess ions distributed diffusely compared to the OHP. The solvated cations in the OHP create an electric field that affects the stability of intermediates in CO_2RR with large dipole moments adsorbed to the electrode.¹³⁵ This resembles ideas from Debye-Hückel theory, which postulates that solvated ions interact with and affect the stability of other charged species in solution.²² Resasco et al. found that the concentration of cations at the OHP increases with increasing cation size.¹³⁵ The increase in cation concentration corresponds to an increase in the current density of HCOO^- and C_2 products for CO_2RR on Cu films, which the authors attributed to hydrated cations stabilizing surface intermediates with large dipole moments (e.g., CO_2^* , CO^* , OCCO^* , OCCHO^*) that lead to these products.¹³⁵ In other words, the cations stabilize CO_2^* relative to CO_2 (decreasing $G_{A^*}^{\ddagger}$ with respect to G_A^{\ddagger}) and increase CO_2^* coverages, impacting HCOO^* and CO^* formation. The cations also lower the free energy of OCCO^* and OCCHO^* more significantly than CO^* , suggesting that the cations stabilize C-C coupling transition states (decreasing G^{\ddagger}) in

comparison to CO^* , leading to a decrease in $\Delta G_{\text{app}}^{\ddagger}$ for the formation of C_2 products from CO^* (Eq. 10). Cations also can affect electrochemical CO reduction (CORR) to hydrocarbon products.¹³⁸⁻¹³⁹ Li et al. demonstrated that Na^+ ions promote the formation of $\text{C}_{\geq 2}$ products,¹³⁸ which they suggested may result from modification of the electric field at the electrode or changes in interfacial water structure. They reasoned that the altered water structure may solvate the C-C coupling transition state more effectively. We propose that hydrated Na^+ in the OHP lower G^{\ddagger} for C-C coupling relative to the system without Na^+ present, thus lowering $\Delta G_{\text{app}}^{\ddagger}$ for $\text{C}_{\geq 2}$ product formation (Eq. 8). In contrast to the changes induced by Na^+ , the Faradaic efficiency of $\text{C}_{\geq 2}$ product formation decreases by a factor of two upon introducing crown ethers.¹³⁸ As illustrated in Fig. 13, crown ethers chelate with Na^+ ions and remove them from the OHP, which prevents the ions from interacting with surface species and likely increases G^{\ddagger} .¹³⁸ In other work, Waegle and co-workers found that the introduction of quaternary alkylammonium cations influenced the selectivity for ethylene formation in CORR in ways that reflected the size of the alkyl substituents.¹³⁹ Ethylene forms in the presence of smaller methyl and ethyl ammonium cations but not for larger propyl and butyl ammonium cations. They showed that the larger cations prevent interfacial water from interacting with adsorbed CO ¹³⁹ and blocks the formation of the CO dimer intermediate for ethylene formation. They postulated that water molecules hydrogen bond to the CO dimer and facilitate its formation. Following this line of thinking, we suggest that water molecules stabilize the transition state for CO dimer formation relative to the adsorbed CO monomers (decreasing G^{\ddagger} in comparison to $G_{A^*}^{\ddagger}$), promoting the ethylene formation pathway. The findings outlined in this paragraph indicate that cations alter the solvent environment at electrode-solvent interfaces, which alters $G_{A^*}^{\ddagger}$ and G^{\ddagger} for CO_2RR and CORR pathways.

Collectively, these contributions show that protic solvents interact with and affect G^{\ddagger} of ionic complexes in solution. The solvent can stabilize ionic additives near active sites, allowing these additives to affect $G_{A^*}^{\ddagger}$ and G^{\ddagger} . Interactions between water and ionic additives influence rates and selectivities for reactions with charged transition states, such as homogeneous alcohol dehydrations and electrocatalytic CO_2RR and CORR. In other instances, solvent molecules may solvate and mobilize a catalytic ion, forming unique catalytic complexes that alter the reaction mechanism. Understanding these interactions enables the rational selection of combinations of ionic additives and solvents to promote desired reaction pathways.

4. Solvents Act as Reactants or Co-Catalysts

A solvent may directly participate as a reactant in a catalytic reaction (Section 4.1). In these cases, reaction rates may not depend strongly on solvent concentration because solvents often exist in large excess relative to reactants. However, the presence and choice of solvent can change the reaction mechanism and affect the identity of reactive species and the relevant standard state free energies (G_A^0 , $G_{A^*}^0$, $G^{0,\ddagger}$) when the solvent forms a reactant. Simultaneously, the solvent may affect G^{\ddagger} of transition

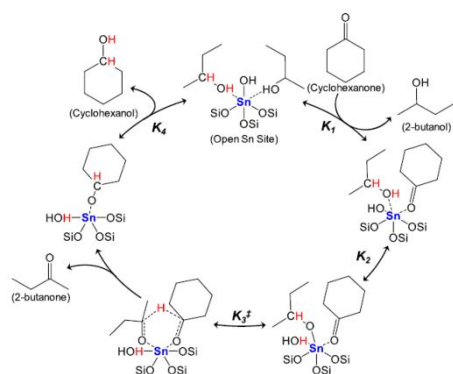


Figure 14. MPVO transfer hydrogenation reaction between cyclohexanone and 2-butanol over Sn-BEA zeolite. Reproduced with permission from Ref. 65. Copyright 2020 American Chemical Society.

states or other reactive species due to intermolecular interactions, including hydrogen bonding and dispersive forces. In addition, solvents may act as co-catalysts by facilitating proton-electron transfer reactions (Section 4.2). By acting as a catalyst, the solvent can introduce a new and more facile reaction pathway than competing reactions in the absence of the solvent. The solvent can also lower G^\ddagger of key transition states and intermediates for this alternate pathway (*Note: a decrease in G^\ddagger represents a change where G^\ddagger becomes more negative; i.e., the species is stabilized*).

4.1 Solvents act as reactants

Solvent molecules can react with reactive solute species or couple to form larger molecules. For example, alcohols act as both solvents and hydrogen donors for catalytic transfer hydrogenation reactions^{65, 140} and serve as the sole reactant for Guerbet alcohol coupling reactions.¹⁴¹⁻¹⁴² Traditional solvents such as ethanol or acetone can also couple with aldehydes in aldol condensation reactions.¹⁴³⁻¹⁴⁴ Non-conventional solvents such as supercritical fluids (i.e., compounds heated beyond their critical point with properties of both liquids and gases) may also function as both a reactant and reaction medium.¹⁴⁵ For example, carbon dioxide hydrogenation¹⁴⁶ and alkene hydroformylation¹⁴⁷ with H_2 proceed efficiently in supercritical carbon dioxide (scCO₂) due to the high solubility of H_2 within scCO₂. Other reactions involving carbon dioxide, including carbonation¹⁴⁸ and copolymerization,¹⁴⁹ sometimes use scCO₂ as a reactant to circumvent organic solvent usage and waste. A decrease in the pressure after the reaction reverts scCO₂ to gaseous CO₂ and allows for easy separation of the products from the solvent. Most of these reactions form products that possess functional groups that resemble the solvent molecule (e.g., ketones, carboxyl groups), but the solvent acts only as a hydrogen donor for catalytic transfer hydrogenations. The hydrogen-donating ability of the solvent is, therefore, an important consideration for transfer hydrogenations.

Catalytic transfer hydrogenations proceed primarily through two mechanisms: a direct hydrogen transfer mechanism known as Meerwein-Ponndorf-Verley reduction and Oppenauer oxidation (MPVO), or an indirect metal hydride route where hydrogen atoms dissociate onto a catalyst surface and serve as the hydrogen source.¹⁴⁰ Transfer hydrogenations with alcohols often involve the MPVO mechanism, which Fig. 14 depicts for the reaction between cyclohexanone and 2-butanol.⁶⁵ Within this mechanism, secondary alcohol solvents lead to greater rates than primary alcohols for the hydrogenation of furfural,¹⁵⁰⁻¹⁵¹ 5-(hydroxymethyl)-furfural,¹⁵¹⁻¹⁵² levulinic acid,¹⁵³ and levulinate esters, among other substrates.¹⁵⁴⁻¹⁵⁶ Some researchers attribute the rate differences to the greater electron-donating ability of the terminal methyl group in secondary alcohols, which leads to greater stabilization of the transition state for methyl levulinate reduction over Hf-, Zr-, Sn-, and Ti-BEA zeolites¹⁵⁴ and furfural hydrogenation over Ru/RuO₂/C.¹⁵⁰ Others argue that secondary alcohols donate hydrogens more efficiently than primary alcohols because a more stable carbocation transition state forms during hydride transfer.¹⁴⁰ Secondary alcohol solvents likely lead to a

lower free energy for the charged hydride transfer transition state ($G^{0,\ddagger}$) compared to the reactants (G_A^0) and a lower ΔG_{app}^\ddagger over comparable intermediates formed from primary alcohols. The dehydrogenation of secondary alcohols also shows greater equilibrium constants than primary alcohols because secondary C-H bonds have lower dissociation energies, which may also affect rates.

In addition to the isomeric structure of the alcohol reactant, the alcohol chain length affects transfer hydrogenation rates. For example, rates decrease with increasing polarity of the alcohol solvent (achieved by decreasing alkyl chain length) for methyl levulinate reduction over Hf-, Zr-, Sn-, and Ti-BEA zeolites¹⁵⁴ and furfural hydrogenation over Ru/RuO₂/C.¹⁵⁰ Panagiotopoulou et al. attributed this effect to stabilizing interactions between more polar solvents and the polar furfural reactant in the liquid phase,¹⁵⁰ while Luo et al. postulated that polar solvents interact more strongly with methyl levulinate derived surface intermediates compared to the transition states.¹⁵⁴ Luo et al. assign the hydride shift between adsorbed solvent and methyl levulinate as the kinetically relevant step; however, reduction rates show a first-order dependence on methyl levulinate concentration,¹⁵⁴ suggesting that the kinetically relevant step involves adsorption of methyl levulinate to the catalyst surface. Interactions between solvent molecules and the reactant in the liquid phase likely explain the trends in both studies discussed here; polar solvents stabilize the polar furfural¹⁵⁰ and methyl levulinate¹⁵⁴ reactants more effectively than less polar solvents, and the decrease in G_A^\ddagger increases ΔG_{app}^\ddagger (Eq. 8) in turn.

These articles demonstrate that liquid and supercritical solvents act as reactants and reaction media for several classes of reactions. In these reactions, the solvent affects G_A^0 , $G_A^{s,0}$, and $G^{0,\ddagger}$ by introducing new reaction pathways and distinct reactive intermediates. For transfer hydrogenation reactions, the solvent can affect the stability of reactants and transition states *via* excess contributions and can directly donate hydrogen atoms to the reactant. In these scenarios, the solvents may simultaneously influence the standard state and excess free energies of key reactive species within the bulk fluid phase and upon the solid catalyst.

4.2 Solvents facilitate proton and electron transfer

Protic solvent molecules facilitate heterolytic oxidation and

transfer to oxygen-derived intermediates (e.g., O_2^* , OOH^* , $H_2O_2^*$, OH^*).¹⁸⁸⁻¹⁹⁰ Those authors suggested that hydrogen molecules dissociate through Heyrovsky-like reactions co-catalyzed by

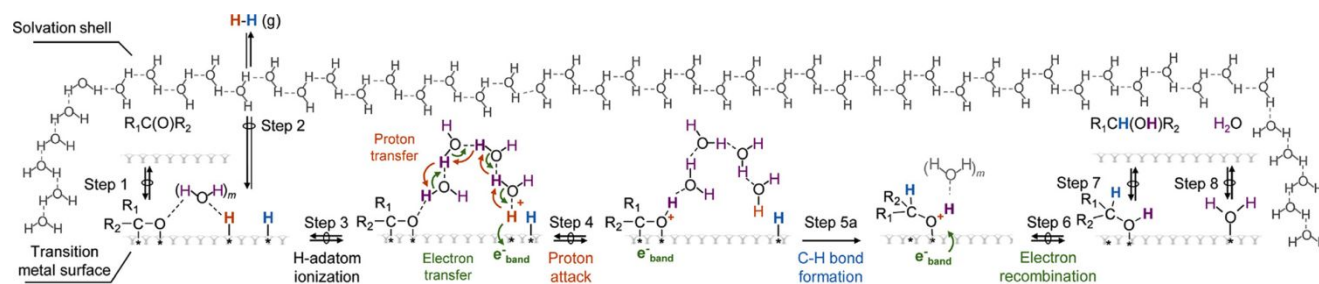


Figure 15. Elementary steps for $R_1C(O)R_2$ hydrogenation via proton-electron transfer (PET) at the H_2O -Ru interface. Reproduced with permission from Ref. 192. Copyright 2019 American Chemical Society.

reduction reactions at the solid-liquid interface of metal nanoparticles. Past studies showed that these proton-electron transfer (PET) reactions occur readily in homogeneous systems¹⁵⁷⁻¹⁵⁹ and on metal catalysts present on electrodes held at an applied potential.¹⁶⁰ Similar PET reactions also influence thermocatalytic processes, which was reflected in observations made by Haruta and co-workers for CO oxidation more than three decades ago but not fully understood at the time.¹⁶¹⁻¹⁶⁴ Their work demonstrated that water increases CO oxidation rates,¹⁶³⁻¹⁶⁵ which Desai and Neurock¹⁶⁶⁻¹⁶⁷ later attributed to water enabling PET for the reaction. Seminal contributions from Chandler and Grabow¹⁶⁸⁻¹⁷⁰ and Iglesia¹⁷¹ further elucidated the effects of water on CO oxidation. Recent reports also showed related phenomena in chemistries such as alcohol oxidation,¹⁷²⁻¹⁷³ carbonyl reduction, hydrodeoxygenation,^{45, 174-176} hydrogen oxidation, and oxygen reduction reactions.¹⁷⁷⁻¹⁸³ In general, these reactions involve coupled or concerted PET steps, in which the solvent shuttles protons from the reductant to activate the oxidant (e.g., O_2 , H_2O_2), while metal nanoparticles and a semiconducting support facilitate electron transfer between the redox pair.

Redox reactions involving O_2 , H_2 , H_2O , and organic oxygenates (e.g., CO) occur readily on metal surfaces and at metal-support interfaces (MSI). A protic solvent molecule solvates reductants bound to the catalyst surface (e.g., H^*), which react to form a proton-electron pair.¹⁸⁴ Many of these reactions involve direct oxidation of H_2 or adsorbed H^* atoms through steps that resemble the Heyrovsky ($H_2 + * + H_2O \rightarrow H^* + H_3O^+ + e^-$) and Volmer ($H^* + H_2O \rightarrow * + H_3O^+ + e^-$) reactions reported in the electrochemical hydrogen oxidation reaction (HOR) literature.¹⁸⁵⁻¹⁸⁷ For example, work from our group on the direct synthesis of H_2O_2 from H_2 and O_2 shows that Pd-, Pt-, and Au-based materials couple HOR with the oxygen reduction reaction (ORR).¹⁷⁷⁻¹⁷⁹ We found that protic solvents are required to achieve detectable rates of H_2O_2 formation.¹⁷⁷ Similarly, rates and selectivities towards H_2O_2 formation increased by an order of magnitude upon increasing the activity of protons by orders of magnitude (e.g., decreasing the pH from 10 to 2), which increase G_A^e relative to $G^{e,\ddagger}$ and thus lower ΔG_{app}^\ddagger to reduce oxygenates.¹⁷⁷ These studies parallel findings by the Chandler and Grabow groups, which show that the MSI of Au nanoparticles and metal-oxide supports (e.g., TiO_2 , Al_2O_3) heterolytically activate hydrogen molecules, leading to electron

hydroxyl groups on the support. DFT calculations and kinetic isotope experiments suggest that heterolytic reactions between hydrogen and oxygen present much lower barriers than competing homolytic surface reactions in the absence of protic solvents.

Analogous PET reactions occur between hydrogen and organic species during the hydrogenation of C-O and C-N bonds. For example, Chin and co-workers reported the promotional role of proton-hydride pairs during gas-phase¹⁸⁴ and liquid phase¹⁹¹⁻¹⁹³ hydrogenation reactions of arene and carbonyl species on Ru-based catalysts. They showed that carbonyl reduction rates increased exponentially with the proton affinity of the carbonyl and the dielectric constant (i.e., a measure of polarity) of the solvent.¹⁹² The authors found that the rate trends and H_2 - D_2 kinetic isotope effects agree more closely with a PET mechanism (shown in Fig. 15) than an alkoxy-based mechanism involving homolytic reactions of H^* .¹⁹² Polar solvents lower $G^{e,\ddagger}$ for the charged carbonyl reduction states more significantly than less polar solvents, leading to the rate increases. Similar work by Zhao et al. indicates that furfural hydrogenation over Pd proceeds by solvent-mediated reactions between H^* and adsorbed intermediates.¹⁹⁴ Reaction rates are orders of magnitude greater in water than cyclohexane, and the dependence of rates on H_2 pressure differs between these solvents.¹⁹⁴ DFT calculations showed that ΔG_{app}^\ddagger decreases by 50-62 kJ mol⁻¹ in the presence of water relative to the vapor phase, which the authors attribute to water facilitating a lower barrier PET pathway to reduce furfural.¹⁹⁴ Water molecules stabilize the positively charged transition state, lowering $G^{e,\ddagger}$ and ΔG_{app}^\ddagger (Eq. 8). For CO hydrogenation over Ru nanoparticles, Hibbitts et al. found that water plays a similar promotional role.¹⁹⁵ Proximal water molecules lower DFT calculated ΔH_{app}^\ddagger values for the reduction of CO^* by allowing for proton transfer in the formation of COH^* and $^*HCOH^*$ intermediates. They postulated that water should lead to greater coverages of $^*HCOH^*$ without affecting chain termination rates. Consequently, water indirectly leads to greater rates of C-C formation during Fischer-Tropsch synthesis by lowering $G^{e,\ddagger}$ for COH^* and $^*HCOH^*$ formation, which increases the selectivity to longer chain hydrocarbon products in comparison to methane.¹⁹⁵ Overall, these studies show that C-O and C-N hydrogenation reactions readily occur via solution-mediated reactions with H^* .

Similar heterolytic processes occur during hydrodeoxygenation (HDO) reactions that cleave C-O bonds in organic oxygenates. Recent experimental and computational studies show that water co-catalyzes HDO reactions over metal surfaces (e.g., Pt, Ni, Ru, and Fe).^{45, 174} For instance, the HDO of phenol¹⁷⁵ and m-cresol¹⁷⁶ over Ru/TiO₂ involves heterolytic activation of H₂ at the MSI between Ru atoms and hydroxyl groups on TiO₂. These reactions involve the formation of proton-hydride pairs consisting of a ruthenium hydride (Ru-H^{δ-}) and a surface-bound water species with an acidic proton (H-O-H^{δ+}).¹⁷⁵⁻¹⁷⁶ The hydride and surface water species facilitate kinetically relevant C-O bond scission by transferring protons across the Ru/TiO₂ interface, which lowers G^{\ddagger} and $\Delta G_{app}^{\ddagger}$ (Eq. 8). Work from the Chin group demonstrated that similar PET reactions occur during the HDO of guaiacol over Ru surfaces.^{193, 196} Beyond serving as a source of protons, water molecules improve selectivity to the desired HDO pathway over the undesired hydrogenation pathway because hydrogen bonding interactions lower G^{\ddagger} for the charged HDO transition state more significantly than the neutral transition state for hydrogenation.¹⁹³ Moreover, the authors indicated that the kinetically relevant C-O bond cleavage occurs through a water-assisted intramolecular PET from the hydroxyl group of guaiacol to the methoxy moiety, while bonding with Ru atoms stabilizes electrons within the aromatic ring.^{193, 196} These investigations suggest that heterolytic solvent-assisted PET processes occur with lower $\Delta G_{app}^{\ddagger}$ than competing homolytic mechanisms and show that excess contributions associated with hydrogen bonding and the permittivity of the solvent influence rates.

Water molecules influence CO transformations through PET processes over metal nanoparticles. For example, CO oxidation and hydrogenation rates increase at low partial pressures of H₂O over Au or Ru nanoparticles supported on metal oxides.^{163-164, 168, 171, 195} Daté et al. also observed that moisture increases CO oxidation rates, and they postulated that water facilitates both O₂ activation¹⁶³⁻¹⁶⁴ and carbonate decomposition,¹⁶⁴ an idea that later studies would corroborate. Several studies showed that an adsorbed water molecule donates a proton to O₂, activating it to form OOH*.^{168-171, 197} Saavedra et al. further demonstrated that CO* and OOH* react to form COOH* species that transfer protons to H₂O during the formation of CO₂.¹⁶⁸ While water can promote CO conversion reactions at low coverages, further increases in water concentration (>100 ppm,¹⁶³ >0.5 kPa¹⁷¹) leads to lower rates, which may result from strong binding and inhibition of active sites by water (as discussed in Section 5.1). Alternatively, water also inhibits catalytic activity for H₂ oxidation over Au/TiO₂,¹⁸⁸⁻¹⁸⁹ which Chandler and co-workers initially attributed to water occupying active sites¹⁸⁸ but later credited to

a monolayer of water on the TiO₂ surface destabilizing the transition state for heterolytic H₂ dissociation and proton transfer to hydroxyl groups on TiO₂ (i.e., increased G^{\ddagger}).¹⁸⁹ Water slows the proton transfer to the hydroxyl group and leads to an accumulation of charge on the Au surface, which increases G^{\ddagger} . The latter explanation may also apply to CO oxidation, where a water monolayer may form at higher water pressures and inhibit proton transfer.

Davis and Neurock found that water facilitates alcohol oxidation and the deprotonation of hydroxylated species over supported Au and Pd catalysts.^{172-173, 198-200} In such systems, glycerol and ethanol oxidation rates increase with the pH of liquid water (i.e., concentrations of OH⁻), which implies that crucial elementary steps involve hydroxide ions.¹⁷²⁻¹⁷³ Isotopic labeling experiments (¹⁸O₂ and H₂¹⁸O) show that the products possess oxygen atoms originating from hydroxide ions or surface hydroxyl groups derived from water and not from molecular oxygen.¹⁷² DFT calculations suggest that these solvent-derived hydroxides and hydroxyl groups offer lower G^{\ddagger} for O-H and C-H bond activation, which reduces $\Delta G_{app}^{\ddagger}$ in comparison to pathways that proceed by dissociative adsorption of the alcohol on these metal surfaces.¹⁷²⁻¹⁷³ Thus, solvents can mediate proton and electron transfer between organic reductants and other oxygen-containing species, lowering $\Delta G_{app}^{\ddagger}$ for kinetically relevant bond activation steps.

Recent work from our group shows that PET processes facilitate multiple elementary steps during the reaction of H₂ and O₂ in the presence of methanol on Pd surfaces (Fig. 16).¹⁸⁰ Specifically, methanol (introduced as the reaction solvent) activates upon Pd surfaces to generate numerous surface species that include hydroxymethyl intermediates (CH₂OH*), which mediate PET steps to O₂* and OOH* species that form H₂O₂ and CH₂O simultaneously.¹⁸⁰ The resulting formaldehyde (CH₂O*) subsequently reacts with hydrogen to regenerate CH₂OH*, analogous to the reactions shown in Fig. 15. Notably, the hydroxymethyl/formaldehyde pair readily transfers both protons and electrons, whereas solution-phase methanol and water molecules transfer only protons effectively. Consequently, DFT calculations reveal that PET pathways that involve CH₂OH* species give significantly lower $\Delta H_{app}^{\ddagger}$ (3-18 kJ mol⁻¹) than solution-mediated pathways (30-33 kJ mol⁻¹). These findings demonstrate that certain oxygenates form surface redox mediators (e.g., CH₂O*/CH₂OH*) that provide alternative paths to co-catalyze PET reactions between distinct redox pairs. Within this system, H₂O₂ formation rates depend strongly on the fractions of methanol and water within the liquid phase and rates reach maximum values in 70 volume % methanol,¹⁸⁰ which indicates that $\Delta G_{app}^{\ddagger}$ for this reaction reaches the minimum value

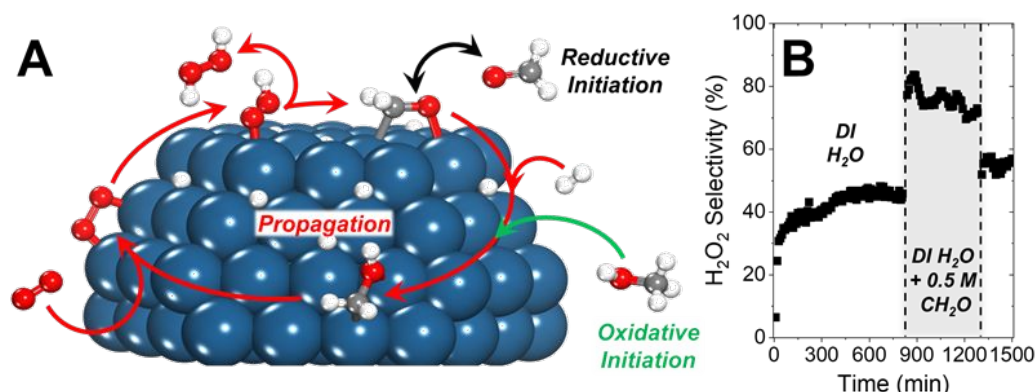


Figure 16. (A) Hydroxymethyl (CH₂OH*) forms either by oxidative initiation of methanol or the reductive initiation of formaldehyde, after which, CH₂OH* acts as a redox mediator for reactions of O₂ and H₂ to form H₂O₂ and water. O atoms are shown in red, H atoms in white, carbon atoms in grey, and Pd atoms in dark blue. (B) Steady-state H₂O₂ selectivities increased when formaldehyde (0.5 M CH₂O) is added to DI H₂O (200 kPa H₂, 60 kPa O₂, 278 K). Adapted from Ref. 180. Reprinted with permission from AAAS.

at this solvent composition. The solvent composition likely affects the solvation of the transition states and intermediates for H_2O_2 formation, leading to changes in G^{\ddagger} and G_A^\ddagger . The observations in this paragraph show that surface species derived from protic solvent molecules facilitate proton-electron transfer and alter ΔG_{app}^\ddagger for H_2O_2 synthesis in similar ways to the oxidation and hydrodeoxygenation processes discussed above.

While Section 3 focuses primarily on the stabilization of reactive species by confined solvent networks or bulk solvent domains, the investigations described here give evidence for catalytic processes that involve direct reactions between reactants and solvent molecules or solvent-derived intermediates. When solvents participate as reactants or co-catalysts, distinct reaction pathways may appear and provide reactive species and transition states with lower standard state free energies (Section 4.1). For example, protic solvent molecules facilitate proton-electron transfer steps that offer lower ΔG_{app}^\ddagger than the pathways that prevail in the absence of a solvent (Section 4.2). The solvent can also lower G^{\ddagger} with respect to G_A^\ddagger and $G_{A^\ddagger}^\ddagger$ for these reactions through hydrogen bonding or electrostatic screening interactions that influence charged transition states. In summary, a significant body of research shows that protic solvents can participate directly in thermocatalytic reactions at solid-liquid interfaces by acting as hydrogen donors or facilitating proton-electron processes.

5. Competition for Active Sites Influences Catalysis

A solvent may inhibit a chemical reaction by competing with reactants for active sites. Researchers recognized this phenomenon decades ago,²⁰¹⁻²⁰⁶ but it remains an important consideration for the design of catalytic processes. The solvent terms introduced to the rate expression in Eq. 13 and 14 quantify the effect of solvent competition on reaction rates. Solvent molecules may directly coordinate to the catalyst active site (Section 5.1) or form hydrogen bonded or otherwise ordered networks that occlude active sites in zeolite pores (Section 5.2). Both situations inhibit reaction rates by reducing the coverage of reactive species. Solvent molecules may also increase G^{\ddagger} by requiring additional energy to desorb from active sites (*Note: an increase in G^\ddagger represents a change where G^\ddagger becomes more positive; i.e., the species is destabilized*).

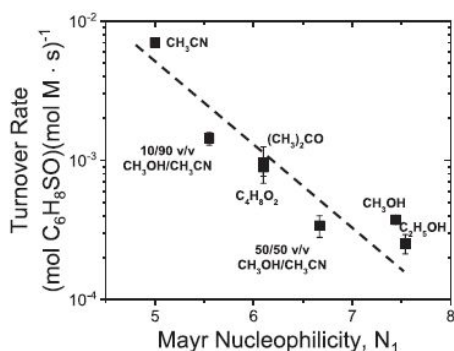


Figure 17. Turnover rates for thiophene oxidation over Ti-BEA zeolite decrease with increasing solvent nucleophilicity, as measured on the Mayr Nucleophilicity scale. Reprinted from Ref. 207, with permission from Elsevier.

5.1 Direct coordination to the active site

Solvents with a high affinity for catalytic surfaces compete with reactants to occupy sites for catalysis. For example, Fig. 17 shows recent work from our group in which thiophene oxidation turnover rates over transition-metal substituted zeolite BEA decrease as the Lewis basicity (i.e., nucleophilicity) of the solvent increases.²⁰⁷ We attributed these trends to coverages of solvent molecules upon Lewis acid active sites that increase with the Lewis base strength of the solvent, which leads to lower coverages of intermediates that participate directly in the catalytic cycle.²⁰⁷ Similarly, rates for the cyclization of citronellal over the Lewis acid catalyst Sn-SBA-15 decrease by an order of magnitude upon changing the solvent from toluene to acetonitrile, which competes with citronellal for the Sn active sites.²⁰⁸ A solvent with a higher affinity for the active metal heteroatom in zeolites will show a greater value of $K_A[S]$ in Eq. 13 and decrease turnover rates.

During reactions on metal surfaces, solvent molecules may reduce the number of available active sites by binding to the surface or affecting the adsorption strength of reactive species. Recent studies by Singh and co-workers demonstrated that the adsorption enthalpies of organics containing hydrogen bonding functions onto Pt²⁰⁹⁻²¹⁰ and Rh²⁰⁹ surfaces are much lower in water than for adsorption from the gas phase to pristine surfaces. Similarly, Yang et al. found that H_2 showed a lower adsorption enthalpy to Pt surfaces in water than in the gas phase.¹²¹ For both cases, the authors attributed the differences to the need to displace water from the surfaces prior to adsorption and the associated enthalpic cost.^{121, 209-210} For the HDO of levulinic acid (LA) over Ru catalysts, Mamun et al. found that 1,4-dioxane adsorbs to the surface more strongly than polar solvents (e.g., methanol, water), which reduces the coverage of LA-derived

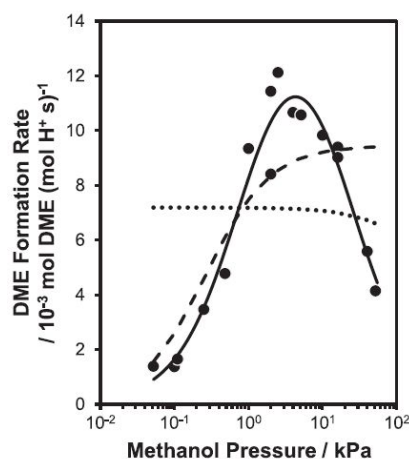


Figure 18. Rates of dimethyl ether formation over H-CHA zeolite increase with methanol pressure at low pressures, then decrease at higher pressures. The solid line represents an associative dehydration rate law with a methanol trimer MASI, the dotted line represents a dissociative rate law with kinetically-relevant methoxy formation and methanol monomers and protonated dimers as the MASI, and the dashed line represents a dissociative rate law with kinetically-relevant DME formation, reversible and quasi-equilibrated methoxy formation, and methanol monomers and protonated dimers as the MASI. Reprinted from Ref. 219, with permission from Elsevier.

intermediates and decreases rates.¹⁰² The rate changes may result

from 1,4-dioxane having a higher affinity for the Ru surface than the polar solvents, but displacing the solvation shell of bulky 1,4-dioxane molecules near the surface may also require a greater energetic penalty than smaller methanol and water molecules. An experimental study on phenol HDO over Pd/C²¹¹ observed that rates vary by solvent choice in the order water > methanol > hexadecane and attributed these results to similar effects as those described by Mamun et al. in reactions of LA. Hexadecane and methanol strongly adsorb to the Pd catalyst surface, leading to lower coverages of reactive species. Referencing the mechanism in Scheme 3, the equilibrium constant for solvent adsorption (K_A) is greater for hexadecane and methanol than water, leading to a decrease in rates. A similar inhibitory effect can occur in the presence of water vapor during gas-phase reactions. As discussed in Section 4, water acts as a co-catalyst for CO oxidation over Au/TiO₂ at low water pressures, but rates decrease at high water pressures.^{163, 171} Daté et al.¹⁶³ and Ojeda et al.¹⁷¹ attributed the rate decreases to water displacing CO and O₂ reactants from active sites at these higher water pressures. Solvent molecules at metal surfaces or nanoparticles can thus increase ΔG^\ddagger_{app} by limiting the access of reactants to active sites.

These reports emphasize the need to consider the direct coordination of solvents (reversible or otherwise) to catalytic sites and the consequences on the number of reactive species for the intended catalytic cycle. An aprotic or protic solvent that binds strongly to a zeolite or metal surface active site can inhibit the reaction by blocking active sites. Solvent molecules can require additional energy to desorb from active sites, which adds to G^\ddagger and lead to an increase in ΔG^\ddagger_{app} .

5.2 Solvent-filled zeolite pores

Solvents may form structured networks within zeolite pores, especially in the cases of protic molecules, that must be displaced or reorganized for reactants to access active sites. Section 3 discussed the excess energy effects of these solvent networks, but here we emphasize how these networks can inhibit access to and competitively bind to active sites. H-MFI zeolites with greater concentrations of Brønsted acid ($H^+(H_2O)_n$) sites (i.e., more hydrophilic) show lower uptakes of cyclohexanol into the pores⁷⁴ and lower rates of cyclohexanol dehydration above 0.4 mmol ($H^+(H_2O)_n$) per gram of MFI.⁷⁵ Pfriem et al. found that the volume between $H^+(H_2O)_n$ clusters reduces to values less than the van der Waals volume of cyclohexanol at high concentrations of $H^+(H_2O)_n$.⁷⁵ These proton-solvent clusters limit the access of cyclohexanol to zeolite pores and decrease cyclohexanol dehydration rates. Separately, the water networks within Ti-BEA-OH pores inhibit aqueous-phase glucose isomerization compared to Ti-BEA-F.^{52, 59} However, not all protic solvents reduce glucose isomerization rates. Methanol⁶³ and ethanol²¹² give greater rates than water for glucose isomerization in Sn-BEA, which the authors attributed to glucose displacing methanol or ethanol molecules more easily than water.^{63, 212} The enthalpies of fusion (ΔH_{fus}) of solvents quantify the strength of hydrogen bonds among molecules, and values for water, methanol, and ethanol are 6.0, 3.2, and 4.9 kJ mol⁻¹, respectively.²¹³ These values relate to ΔG^\ddagger_{app} and, by extension, the respective differences between glucose

isomerization rates in solvent-filled pores of Sn-BEA zeolites. Solvents that show a larger ΔH_{fus} presumably require greater energy to be disrupted or displaced, which leads to an increase in ΔG^\ddagger_{app} and lower rates.

The presence of a protic solvent can also limit rates in gas-phase reactions. When water vapor is co-fed with reactants, increasing the water pressure decreases reaction rates for zeolite catalyzed cyclohexene epoxidation,²¹⁴ ethanol dehydration,²¹⁵⁻²¹⁶ 1-propanol dehydration,²¹⁷ and methyl lactate dehydration.²¹⁸ Some authors assign this effect to competitive adsorption of water to active sites (Scheme 3),^{214-215, 218} while others reason that water stabilizes reactive intermediates more significantly than kinetically relevant transition states (increasing ΔG^\ddagger_{app}).²¹⁷ Similarly, protic reactants can inhibit a zeolite catalyzed reaction as reactant pressures increase. For 1-propanol dehydration over H-MFI, the rate of monomolecular dehydration decreases with increasing 1-propanol pressure, while the rate of bimolecular dehydration increases due to preferential formation of 1-propanol dimers at higher pressures.²¹⁷ A separate study on bimolecular methanol dehydration over H-CHA found that rates of dimethyl ether (DME) formation initially increase with methanol pressure but decrease with a superlinear dependence on methanol pressure at the highest values (Fig. 18).²¹⁹ Dehydration proceeds through a dissociative mechanism (represented by the dashed line in Fig. 18) at low methanol pressures (<4 kPa). This process involves adsorbed and protonated methanol ($CH_3OH_2^{+*}$) undergoing kinetically relevant dehydration to eliminate H₂O and form a methyl intermediate (CH_3^*) that reacts with a gas-phase methanol molecule to form DME. At higher methanol pressures (>4 kPa), dehydration preferentially occurs by an associative mechanism (represented by the solid line in Fig. 18) in which DME forms in the kinetically relevant step from a methanol trimer that contains one spectator methanol. At methanol pressures above 10 kPa, the authors argue that methanol tetramers and pentamers gather at the active site and 2-3 spectator methanol molecules must be displaced by the bimolecular transition state that yields the ether.²¹⁹ The presence of these additional spectator methanol molecules inhibits the associative pathway with increasing methanol pressures. The extended methanol complexes that form at higher pressures likely approached the condensed phase structures in zeolite pores in a liquid phase reaction. The complexes likely increase ΔG^\ddagger_{app} by introducing an energetic penalty for adsorbing reactants.

Collectively, the studies discussed in this section demonstrate that solvents can inhibit catalytic reactions by indirect or direct interaction with the active site. An aprotic or protic solvent with a high affinity for active sites within a zeolite or on a metal surface may directly coordinate to that site and prevent reactants from binding. A protic solvent may also form an extended hydrogen bonded network in a zeolite pore that may inhibit adsorption without directly interacting with the active site. These inhibitory effects can increase ΔG^\ddagger_{app} , meaning that solvent competition can significantly affect catalysis and warrants consideration for liquid phase systems.

6. Conclusions and Future Outlook

Solvent interactions with reactants and active sites can drastically affect the rate and selectivity of chemical reactions, which makes the choice of solvent a critical consideration when creating catalysts or designing processes. The specificity of these interactions implies that a solvent that provides optimal catalytic properties for a certain pairing of reactants and a catalyst may be suboptimal following seemingly innocuous changes in the extended surface of the catalyst or the distal end of the reactant. To explain the origins of these effects, we presented rate expressions and equations that quantify the effect of solvents on reaction rates (Section 2). We then used those generalizable frameworks to connect studies in which solvent molecules affect G^\ddagger of reactive species by solvation (Section 3), act as a reactant or co-catalyst and directly participate in chemical reactions (Section 4), and competitively bind to active sites and inhibit reactions (Section 5). These simple models show that an optimal solvent minimizes ΔG_{app}^\ddagger for desired reactions by altering the G^\ddagger of reactive species or introduces new mechanisms and reaction pathways. Developing effective combinations of reactant, solvent, and catalyst requires a molecular understanding of the interactions between these three components at solid-liquid interfaces.

Investigations conducted over the past 150 years repeatedly illustrate the ability of solvents to impact rates and selectivities of chemical reactions, but only recently have these studies begun to elucidate molecularly informed explanations for these kinetic changes. Theoretical treatments, such as transition state theory and microkinetic modeling, can identify the impact of solvents on the energetics of reaction steps and the stability of reactive species. Experimental techniques, including infrared and nuclear magnetic resonance spectroscopy, allow for direct observation of solvent structures and binding configurations with reactants or catalytic functions. Computational efforts, namely MD simulations and DFT, can provide molecular detail of solvent interactions with reactants and catalysts and support experimentally calculated changes in G^\ddagger . The insights gained from these techniques can be coupled with machine learning to develop quantitative structure-activity relationships that may predict solvent effects and identify methods to more effectively combine reactants, solvents, and catalysts to selectively form desired molecules.

This contribution summarizes recent efforts to interpret solvent effects at the molecular level. Many industrial processes must occur at mild conditions in a solvent, which yields an extensive carbon footprint.²²⁰ Understanding how solvents influence reactions is critical to improving the efficiency of these processes and reducing waste. The findings discussed here represent ongoing work from many groups, including our own, to elucidate how unique solvent structures affect liquid- and gas-phase catalytic reactions. The catalysis community must develop a more comprehensive understanding of solvent-mediated interactions to truly design solid-liquid interfaces that select reactive intermediates or transition states based on intermolecular forces beyond those present at the point of covalent attachment.

Author Contributions

We strongly encourage authors to include author contributions and recommend using [CRedit](#) for standardised contribution descriptions. Please refer to our general [author guidelines](#) for more information about authorship.

Conflicts of interest

There are no conflicts to declare.

Acknowledgments

The authors acknowledge insightful and enjoyable discussions of these topics with Profs. Matthew Neurock, Justin Notestein, Joaquín Rodríguez-López, Rajamani Gounder, Enrique Iglesia, David Hibbitts, and Diwakar Shukla. This work was supported by the Department of Energy (DE-SC0010224). J.S.A., D.S.P., and C.T. acknowledge the National Science Foundation Graduate Research Fellowship program (DGE-1144245 and DGE-1746047).

Notes and references

- Norskov, J. K.; Abild-Pedersen, F.; Studt, F.; Bligaard, T., Density functional theory in surface chemistry and catalysis. *Proceedings of the National Academy of Sciences* **2011**, *108* (3), 937-943.
- Vojvodic, A.; Norskov, J. K.; Abild-Pedersen, F., Electronic Structure Effects in Transition Metal Surface Chemistry. *Topics in Catalysis* **2014**, *57* (1-4), 25-32.
- Yu, W.; Porosoff, M. D.; Chen, J. G., Review of Pt-Based Bimetallic Catalysis: From Model Surfaces to Supported Catalysts. *Chemical Reviews* **2012**, *112* (11), 5780-5817.
- Cornils, B.; Herrmann, W. A.; Beller, M.; Paciello, R., *Applied homogeneous catalysis with organometallic compounds: a comprehensive handbook in four volumes*. John Wiley & Sons: 2017; Vol. 4.
- Blakemore, J. D.; Crabtree, R. H.; Brudvig, G. W., Molecular Catalysts for Water Oxidation. *Chemical Reviews* **2015**, *115* (23), 12974-13005.
- Mukherjee, A.; Milstein, D., Homogeneous Catalysis by Cobalt and Manganese Pincer Complexes. *ACS Catalysis* **2018**, *8* (12), 11435-11469.
- Mehta, P.; Barboun, P.; Go, D. B.; Hicks, J. C.; Schneider, W. F., Catalysis Enabled by Plasma Activation of Strong Chemical Bonds: A Review. *ACS Energy Letters* **2019**, *4* (5), 1115-1133.
- Hong, J.; Praver, S.; Murphy, A. B., Plasma Catalysis as an Alternative Route for Ammonia Production: Status, Mechanisms, and Prospects for Progress. *ACS Sustainable Chemistry & Engineering* **2018**, *6* (1), 15-31.
- Mehta, P.; Barboun, P.; Herrera, F. A.; Kim, J.; Rumbach, P.; Go, D. B.; Hicks, J. C.; Schneider, W. F., Overcoming ammonia synthesis scaling relations with plasma-enabled catalysis. *Nature Catalysis* **2018**, *1* (4), 269-275.
- Sheldon, R., Catalytic reactions in ionic liquids. *Chemical Communications* **2001**, (23), 2399-2407.
- Pârvulescu, V. I.; Hardacre, C., Catalysis in Ionic Liquids. *Chemical Reviews* **2007**, *107* (6), 2615-2665.
- Berzelius, J., Quelques Idées sur une nouvelle Force agissant dans les Combinaisons des Corps Organiques. *Annali di Chimica* **1836**, *61*, 146-151.

13. Ayla, E. Z.; Potts, D. S.; Bregante, D. T.; Flaherty, D. W., Alkene Epoxidations with H₂O₂ over Groups 4–6 Metal-Substituted BEA Zeolites: Reactive Intermediates, Reaction Pathways, and Linear Free-Energy Relationships. *ACS Catalysis* **2021**, *11* (1), 139-154.
14. Bregante, D. T.; Flaherty, D. W., Periodic Trends in Olefin Epoxidation over Group IV and V Framework-Substituted Zeolite Catalysts: A Kinetic and Spectroscopic Study. *Journal of the American Chemical Society* **2017**, *139* (20), 6888-6898.
15. Bregante, D. T.; Thornburg, N. E.; Notestein, J. M.; Flaherty, D. W., Consequences of Confinement for Alkene Epoxidation with Hydrogen Peroxide on Highly Dispersed Group 4 and 5 Metal Oxide Catalysts. *ACS Catalysis* **2018**, *8* (4), 2995-3010.
16. Yun, D.; Ayla, E. Z.; Bregante, D. T.; Flaherty, D. W., Reactive Species and Reaction Pathways for the Oxidative Cleavage of 4-Octene and Oleic Acid with H₂O₂ over Tungsten Oxide Catalysts. *ACS Catalysis* **2021**, *11* (5), 3137-3152.
17. Ghosh, T. K.; Nair, N. N., Rh^{1/γ}-Al₂O₃ Single-Atom Catalysis of O₂ Activation and CO Oxidation: Mechanism, Effects of Hydration, Oxidation State, and Cluster Size. *ChemCatChem* **2013**, *5* (7), 1811-1821.
18. Guzman, J.; Gates, B. C., Catalysis by Supported Gold: Correlation between Catalytic Activity for CO Oxidation and Oxidation States of Gold. *Journal of the American Chemical Society* **2004**, *126* (9), 2672-2673.
19. Menshutkin, N., Über die Affinitätskoeffizienten der Alkylhaloide und der Amine. *Zeitschrift für Physikalische Chemie* **1890**, *6* (1), 41.
20. Dyson, P. J.; Jessop, P. G., Solvent effects in catalysis: rational improvements of catalysts via manipulation of solvent interactions. *Catalysis Science & Technology* **2016**, *6* (10), 3302-3316.
21. Reichardt, C.; Welton, T., *Solvents and solvent effects in organic chemistry*. John Wiley & Sons: 2011.
22. Debye, P. H., E., Zur Theorie der Elektrolyte. I. Gefrierpunktniedrigung und verwandte Erscheinungen. *Physikalische Zeitschrift* **1923**, *24* (9), 185-206.
23. Kamlet, M. J.; Abboud, J. L. M.; Abraham, M. H.; Taft, R. W., Linear solvation energy relationships. 23. A comprehensive collection of the solvatochromic parameters, .pi.*, .alpha., and .beta., and some methods for simplifying the generalized solvatochromic equation. *The Journal of Organic Chemistry* **1983**, *48* (17), 2877-2887.
24. Kirkwood, J. G., Theory of Solutions of Molecules Containing Widely Separated Charges with Special Application to Zwitterions. *The Journal of Chemical Physics* **1934**, *2* (7), 351-361.
25. Gould, N. S.; Xu, B., Catalyst characterization in the presence of solvent: development of liquid phase structure–activity relationships. *Chemical Science* **2018**, *9* (2), 281-287.
26. Sievers, C.; Noda, Y.; Qi, L.; Albuquerque, E. M.; Rioux, R. M.; Scott, S. L., Phenomena Affecting Catalytic Reactions at Solid–Liquid Interfaces. *ACS Catalysis* **2016**, *6* (12), 8286-8307.
27. Harris, J. W.; Bates, J. S.; Bukowski, B. C.; Greeley, J.; Gounder, R., Opportunities in Catalysis over Metal-Zeotypes Enabled by Descriptions of Active Centers Beyond Their Binding Site. *ACS Catalysis* **2020**, *10* (16), 9476-9495.
28. Bates, J. S.; Gounder, R., Kinetic effects of molecular clustering and solvation by extended networks in zeolite acid catalysis. *Chemical Science* **2021**, *12* (13), 4699-4708.
29. Li, G.; Wang, B.; Resasco, D. E., Water-Mediated Heterogeneously Catalyzed Reactions. *ACS Catalysis* **2020**, *10* (2), 1294-1309.
30. Stanciakova, K.; Weckhuysen, B. M., Water–active site interactions in zeolites and their relevance in catalysis. *Trends in Chemistry* **2021**, *3* (6), 456-468.
31. Dimitratos, N.; Lopez-Sanchez, J. A.; Hutchings, G. J., Selective liquid phase oxidation with supported metal nanoparticles. *Chem. Sci.* **2012**, *3* (1), 20-44.
32. Blakemore, D. C.; Castro, L.; Churcher, I.; Rees, D. C.; Thomas, A. W.; Wilson, D. M.; Wood, A., Organic synthesis provides opportunities to transform drug discovery. *Nature Chemistry* **2018**, *10* (4), 383-394.
33. Eyring, H., The Activated Complex and the Absolute Rate of Chemical Reactions. *Chemical Reviews* **1935**, *17* (1), 65-77.
34. Madon, R. J.; Iglesia, E., Catalytic reaction rates in thermodynamically non-ideal systems. *Journal of Molecular Catalysis A: Chemical* **2000**, *163* (1-2), 189-204.
35. Noh, G.; Shi, Z.; Zones, S. I.; Iglesia, E., Isomerization and β-scission reactions of alkanes on bifunctional metal-acid catalysts: Consequences of confinement and diffusional constraints on reactivity and selectivity. *Journal of Catalysis* **2018**, *368*, 389-410.
36. Gounder, R.; Iglesia, E., The catalytic diversity of zeolites: confinement and solvation effects within voids of molecular dimensions. *Chemical Communications* **2013**, *49* (34), 3491-3509.
37. Jones, A. J.; Zones, S. I.; Iglesia, E., Implications of Transition State Confinement within Small Voids for Acid Catalysis. *The Journal of Physical Chemistry C* **2014**, *118* (31), 17787-17800.
38. Rodriguez-Reyes, J. C. F.; Siler, C. G. F.; Liu, W.; Tkatchenko, A.; Friend, C. M.; Madix, R. J., van der Waals Interactions Determine Selectivity in Catalysis by Metallic Gold. *Journal of the American Chemical Society* **2014**, *136* (38), 13333-13340.
39. Karakalos, S.; Xu, Y.; Cheenicode Kabeer, F.; Chen, W.; Rodríguez-Reyes, J. C. F.; Tkatchenko, A.; Kaxiras, E.; Madix, R. J.; Friend, C. M., Noncovalent Bonding Controls Selectivity in Heterogeneous Catalysis: Coupling Reactions on Gold. *Journal of the American Chemical Society* **2016**, *138* (46), 15243-15250.
40. Derita, L.; Dai, S.; Lopez-Zepeda, K.; Pham, N.; Graham, G. W.; Pan, X.; Christopher, P., Catalyst Architecture for Stable Single Atom Dispersion Enables Site-Specific Spectroscopic and Reactivity Measurements of CO Adsorbed to Pt Atoms, Oxidized Pt Clusters, and Metallic Pt Clusters on TiO₂. *Journal of the American Chemical Society* **2017**, *139* (40), 14150-14165.
41. Abrams, D. S.; Prausnitz, J. M., Statistical thermodynamics of liquid mixtures: A new expression for the excess Gibbs energy of partly or completely miscible systems. *AIChE Journal* **1975**, *21* (1), 116-128.
42. Renon, H.; Prausnitz, J. M., Local compositions in thermodynamic excess functions for liquid mixtures. *AIChE Journal* **1968**, *14* (1), 135-144.
43. Wilson, G. M., Vapor-Liquid Equilibrium. XI. A New Expression for the Excess Free Energy of Mixing. *Journal of the American Chemical Society* **1964**, *86* (2), 127-130.
44. Agmon, N., The Grotthuss mechanism. *Chemical Physics Letters* **1995**, *244* (5-6), 456-462.
45. Yoon, Y.; Rousseau, R.; Weber, R. S.; Mei, D.; Lercher, J. A., First-Principles Study of Phenol Hydrogenation on Pt and Ni Catalysts in Aqueous Phase. *Journal of the American Chemical Society* **2014**, *136* (29), 10287-10298.
46. Bregante, D. T.; Johnson, A. M.; Patel, A. Y.; Ayla, E. Z.; Cordon, M. J.; Bukowski, B. C.; Greeley, J.; Gounder, R.; Flaherty, D. W., Cooperative Effects between Hydrophilic Pores and Solvents: Catalytic Consequences of Hydrogen Bonding on Alkene Epoxidation in Zeolites. *Journal of the American Chemical Society* **2019**, *141*, 7302-7319.
47. Bregante, D. T.; Chan, M.; Tan, J. Z.; Ayla, E. Z.; Nicholas, C. P.; Shukla, D.; Flaherty, D. W., The Shape of Water in Zeolites and its Impact on Epoxidation Catalysis. *Nature Catalysis* **2021**, *in press*.

48. Wu, L.; Tang, Z.; Yu, Y.; Yao, X.; Liu, W.; Li, L.; Yan, B.; Liu, Y.; He, M., Facile synthesis of a high-performance titanosilicate catalyst with controllable defective Ti(OSi)3OH sites. *Chemical Communications* **2018**, *54* (49), 6384-6387.
49. Tang, Z.; Yu, Y.; Liu, W.; Chen, Z.; Wang, R.; Liu, H.; Wu, H.; Liu, Y.; He, M., Deboronation-assisted construction of defective Ti(OSi)3OH species in MWW-type titanosilicate and their enhanced catalytic performance. *Catalysis Science & Technology* **2020**, *10* (9), 2905-2915.
50. Wang, L.; Sun, J.; Meng, X.; Zhang, W.; Zhang, J.; Pan, S.; Shen, Z.; Xiao, F. S., A significant enhancement of catalytic activities in oxidation with H₂O₂ over the TS-1 zeolite by adjusting the catalyst wettability. *Chem Commun (Camb)* **2014**, *50* (16), 2012-4.
51. Bregante, D. T.; Potts, D. S.; Kwon, O.; Ayla, E. Z.; Tan, J. Z.; Flaherty, D. W., Effects of Hydrofluoric Acid Concentration on the Density of Silanol Groups and Water Adsorption in Hydrothermally Synthesized Transition-Metal-Substituted Silicalite-1. *Chemistry of Materials* **2020**, *32* (17), 7425-7437.
52. Gounder, R.; Davis, M. E., Beyond shape selective catalysis with zeolites: Hydrophobic void spaces in zeolites enable catalysis in liquid water. *AIChE Journal* **2013**, *59* (9), 3349-3358.
53. Grosso-Giordano, N. A.; Schroeder, C.; Okrut, A.; Solovyov, A.; Schöttle, C.; Chassé, W.; Marinković, N.; Koller, H.; Zones, S. I.; Katz, A., Outer-Sphere Control of Catalysis on Surfaces: A Comparative Study of Ti(IV) Single-Sites Grafted on Amorphous versus Crystalline Silicates for Alkene Epoxidation. *Journal of the American Chemical Society* **2018**, *140* (15), 4956-4960.
54. Grosso-Giordano, N. A.; Hoffman, A. S.; Boubnov, A.; Small, D. W.; Bare, S. R.; Zones, S. I.; Katz, A., Dynamic Reorganization and Confinement of TiIV Active Sites Controls Olefin Epoxidation Catalysis on Two-Dimensional Zeotypes. *Journal of the American Chemical Society* **2019**, *141* (17), 7090-7106.
55. Wang, L.; Sun, J.; Meng, X.; Zhang, W.; Zhang, J.; Pan, S.; Shen, Z.; Xiao, F.-S., A significant enhancement of catalytic activities in oxidation with H₂O₂ over the TS-1 zeolite by adjusting the catalyst wettability. *Chemical Communications* **2014**, *50* (16), 2012-2014.
56. Bregante, D. T.; Flaherty, D. W., Impact of Specific Interactions Among Reactive Surface Intermediates and Confined Water on Epoxidation Catalysis and Adsorption in Lewis Acid Zeolites. *ACS Catalysis* **2019**, *9* (12), 10951-10962.
57. Harris, J. W.; Cordon, M. J.; Di Iorio, J. R.; Vega-Vila, J. C.; Ribeiro, F. H.; Gounder, R., Titration and quantification of open and closed Lewis acid sites in Sn-Beta zeolites that catalyze glucose isomerization. *Journal of Catalysis* **2016**, *335*, 141-154.
58. Vega-Vila, J. C.; Harris, J. W.; Gounder, R., Controlled insertion of tin atoms into zeolite framework vacancies and consequences for glucose isomerization catalysis. *Journal of Catalysis* **2016**, *344*, 108-120.
59. Cordon, M. J.; Harris, J. W.; Vega-Vila, J. C.; Bates, J. S.; Kaur, S.; Gupta, M.; Witzke, M. E.; Wegener, E. C.; Miller, J. T.; Flaherty, D. W.; Hibbitts, D. D.; Gounder, R., Dominant Role of Entropy in Stabilizing Sugar Isomerization Transition States within Hydrophobic Zeolite Pores. *Journal of the American Chemical Society* **2018**, *140* (43), 14244-14266.
60. Cordon, M. J.; Hall, J. N.; Harris, J. W.; Bates, J. S.; Hwang, S.-J.; Gounder, R., Deactivation of Sn-Beta zeolites caused by structural transformation of hydrophobic to hydrophilic micropores during aqueous-phase glucose isomerization. *Catalysis Science & Technology* **2019**, *9* (7), 1654-1668.
61. Gounder, R.; Davis, M. E., Monosaccharide and disaccharide isomerization over Lewis acid sites in hydrophobic and hydrophilic molecular sieves. *Journal of Catalysis* **2013**, *308*, 176-188.
62. Bermejo-Deval, R.; Orazov, M.; Gounder, R.; Hwang, S.-J.; Davis, M. E., Active Sites in Sn-Beta for Glucose Isomerization to Fructose and Epimerization to Mannose. *ACS Catalysis* **2014**, *4* (7), 2288-2297.
63. Christianson, J. R.; Caratzoulas, S.; Vlachos, D. G., Computational Insight into the Effect of Sn-Beta Na Exchange and Solvent on Glucose Isomerization and Epimerization. *ACS Catalysis* **2015**, *5* (9), 5256-5263.
64. Vega-Vila, J. C.; Gounder, R., Quantification of Intraporous Hydrophilic Binding Sites in Lewis Acid Zeolites and Consequences for Sugar Isomerization Catalysis. *ACS Catalysis* **2020**, *10* (20), 12197-12211.
65. Di Iorio, J. R.; Johnson, B. A.; Román-Leshkov, Y., Ordered Hydrogen-Bonded Alcohol Networks Confined in Lewis Acid Zeolites Accelerate Transfer Hydrogenation Turnover Rates. *Journal of the American Chemical Society* **2020**, *142* (45), 19379-19392.
66. Tan, J. Z.; Bregante, D. T.; Torres, C.; Flaherty, D. W., Transition State Stabilization Depends on Solvent Identity, Pore Size, and Hydrophilicity for Epoxidations in Zeolites. *Submitted*.
67. Wang, M.; Jaegers, N. R.; Lee, M.-S.; Wan, C.; Hu, J. Z.; Shi, H.; Mei, D.; Burton, S. D.; Camaioni, D. M.; Gutierrez, O. Y.; Glezakou, V.-A.; Rousseau, R.; Wang, Y.; Lercher, J. A., Genesis and Stability of Hydronium Ions in Zeolite Channels. *J. Am. Chem. Soc.* **2019**, *141*, 3444-3455.
68. Wang, M.; Jaegers, N. R.; Lee, M. S.; Wan, C.; Hu, J. Z.; Shi, H.; Mei, D.; Burton, S. D.; Camaioni, D. M.; Gutierrez, O. Y.; Glezakou, V. A.; Rousseau, R.; Wang, Y.; Lercher, J. A., Genesis and Stability of Hydronium Ions in Zeolite Channels. *J Am Chem Soc* **2019**, *141* (8), 3444-3455.
69. Bates, J. S.; Bukowski, B. C.; Greeley, J.; Gounder, R., Structure and solvation of confined water and water-ethanol clusters within microporous Brønsted acids and their effects on ethanol dehydration catalysis. *Chemical Science* **2020**, *11* (27), 7102-7122.
70. Liu, Y.; Vjunov, A.; Shi, H.; Eckstein, S.; Camaioni, D. M.; Mei, D.; Baráth, E.; Lercher, J. A., Enhancing the catalytic activity of hydronium ions through constrained environments. *Nature Communications* **2017**, *8* (1), 14113.
71. Shi, H.; Eckstein, S.; Vjunov, A.; Camaioni, D. M.; Lercher, J. A., Tailoring nanoscopic confines to maximize catalytic activity of hydronium ions. *Nature Communications* **2017**, *8* (1), 15442.
72. Shetty, M.; Wang, H.; Chen, F.; Jaegers, N.; Liu, Y.; Camaioni, D. M.; Gutiérrez, O. Y.; Lercher, J. A., Directing the Rate-Enhancement for Hydronium Ion Catalyzed Dehydration via Organization of Alkanols in Nanoscopic Confinements. *Angewandte Chemie International Edition* **2021**, *60* (5), 2304-2311.
73. Milakovic, L.; Hintermeier, P. H.; Liu, Q.; Shi, H.; Liu, Y.; Baráth, E.; Lercher, J. A., Towards understanding and predicting the hydronium ion catalyzed dehydration of cyclic-primary, secondary and tertiary alcohols. *Journal of Catalysis* **2020**, *390*, 237-243.
74. Eckstein, S.; Hintermeier, P. H.; Zhao, R.; Baráth, E.; Shi, H.; Liu, Y.; Lercher, J. A., Influence of Hydronium Ions in Zeolites on Sorption. *Angewandte Chemie International Edition* **2019**, *58* (11), 3450-3455.
75. Pfriem, N.; Hintermeier, P. H.; Eckstein, S.; Kim, S.; Liu, Q.; Shi, H.; Milakovic, L.; Liu, Y.; Haller, G. L.; Baráth, E.; Liu, Y.; Lercher, J. A., Role of the ionic environment in enhancing the activity of reacting molecules in zeolite pores. *Science* **2021**, eabh3418.
76. Chen, F.; Shetty, M.; Wang, M.; Shi, H.; Liu, Y.; Camaioni, D. M.; Gutiérrez, O. Y.; Lercher, J. A., Differences in Mechanism and Rate of Zeolite-Catalyzed Cyclohexanol Dehydration in Apolar and Aqueous Phase. *ACS Catalysis* **2021**, *11* (5), 2879-2888.
77. Liu, Y.; Baráth, E.; Shi, H.; Hu, J.; Camaioni, D. M.; Lercher, J. A., Solvent-determined mechanistic pathways in zeolite-H-BEA-catalysed phenol alkylation. *Nature Catalysis* **2018**, *1* (2), 141-147.

78. Bregante, D. T.; Tan, J. Z.; Sutrisno, A.; Flaherty, D. W., Heteroatom substituted zeolite FAU with ultralow Al contents for liquid-phase oxidation catalysis. *Catalysis Science & Technology* **2020**, *10* (3), 635-647.
79. Bregante, D. T.; Tan, J. Z.; Schultz, R. L.; Ayla, E. Z.; Potts, D. S.; Torres, C.; Flaherty, D. W., Catalytic Consequences of Oxidant, Alkene, and Pore Structures on Alkene Epoxidations within Titanium Silicates. *ACS Catalysis* **2020**, *10* (17), 10169-10184.
80. Mellmer, M. A.; Sener, C.; Gallo, J. M.; Luterbacher, J. S.; Alonso, D. M.; Dumesic, J. A., Solvent effects in acid-catalyzed biomass conversion reactions. *Angewandte Chemie International Edition* **2014**, *53* (44), 11872-11875.
81. Mellmer, M. A.; Sanpitakseree, C.; Demir, B.; Bai, P.; Ma, K.; Neurock, M.; Dumesic, J. A., Solvent-enabled control of reactivity for liquid-phase reactions of biomass-derived compounds. *Nature Catalysis* **2018**, *1* (3), 199-207.
82. Mellmer, M. A.; Sanpitakseree, C.; Demir, B.; Ma, K.; Elliott, W. A.; Bai, P.; Johnson, R. L.; Walker, T. W.; Shanks, B. H.; Rioux, R. M.; Neurock, M.; Dumesic, J. A., Effects of chloride ions in acid-catalyzed biomass dehydration reactions in polar aprotic solvents. *Nature Communications* **2019**, *10* (1), 1132.
83. Walker, T. W.; Chew, A. K.; Li, H.; Demir, B.; Zhang, Z. C.; Huber, G. W.; Van Lehn, R. C.; Dumesic, J. A., Universal kinetic solvent effects in acid-catalyzed reactions of biomass-derived oxygenates. *Energy & Environmental Science* **2018**, *11* (3), 617-628.
84. Chew, A. K.; Van Lehn, R. C., Quantifying the Stability of the Hydronium Ion in Organic Solvents With Molecular Dynamics Simulations. *Frontiers in Chemistry* **2019**, *7*.
85. Chew, A. K.; Walker, T. W.; Shen, Z.; Demir, B.; Witteman, L.; Euclide, J.; Huber, G. W.; Dumesic, J. A.; Van Lehn, R. C., Effect of Mixed-Solvent Environments on the Selectivity of Acid-Catalyzed Dehydration Reactions. *ACS Catalysis* **2019**, *10* (3), 1679-1691.
86. Mostofian, B.; Cai, C. M.; Smith, M. D.; Petridis, L.; Cheng, X.; Wyman, C. E.; Smith, J. C., Local Phase Separation of Co-solvents Enhances Pretreatment of Biomass for Bioenergy Applications. *Journal of the American Chemical Society* **2016**, *138* (34), 10869-10878.
87. Cai, C. M.; Nagane, N.; Kumar, R.; Wyman, C. E., Coupling metal halides with a co-solvent to produce furfural and 5-HMF at high yields directly from lignocellulosic biomass as an integrated biofuels strategy. *Green Chemistry* **2014**, *16* (8), 3819-3829.
88. Mellmer, M. A.; Gallo, J. M. R.; Martin Alonso, D.; Dumesic, J. A., Selective Production of Levulinic Acid from Furfuryl Alcohol in THF Solvent Systems over H-ZSM-5. *ACS Catalysis* **2015**, *5* (6), 3354-3359.
89. Qi, L.; Alamillo, R.; Elliott, W. A.; Andersen, A.; Hoyt, D. W.; Walter, E. D.; Han, K. S.; Washton, N. M.; Rioux, R. M.; Dumesic, J. A.; Scott, S. L., Operando Solid-State NMR Observation of Solvent-Mediated Adsorption-Reaction of Carbohydrates in Zeolites. *ACS Catalysis* **2017**, 3489-3500.
90. Zaitseva, A.; Pokki, J.-P.; Le, H. Q.; Alopaeus, V.; Sixta, H., Vapor-Liquid Equilibria, Excess Enthalpy, and Density of Aqueous γ -Valerolactone Solutions. *Journal of Chemical & Engineering Data* **2016**, *61* (2), 881-890.
91. Chou, B.; Tsai, J.-L.; Cheng, S., Cu-substituted molecular sieves as liquid phase oxidation catalysts. *Microporous and Mesoporous Materials* **2001**, *48* (1-3), 309-317.
92. Agirrezabal-Telleria, I.; Iglesia, E., Mechanistic insights and consequences of intrapore liquids in ethene, propene, and butene dimerization on isolated Ni²⁺ sites grafted within aluminosilicate mesopores. *Journal of Catalysis* **2020**, *389*, 690-705.
93. Agirrezabal-Telleria, I.; Iglesia, E., Stabilization of active, selective, and regenerable Ni-based dimerization catalysts by condensation of ethene within ordered mesopores. *Journal of Catalysis* **2017**, *352*, 505-514.
94. Madrahimov, S. T.; Gallagher, J. R.; Zhang, G.; Meinhart, Z.; Garibay, S. J.; Delferro, M.; Miller, J. T.; Farha, O. K.; Hupp, J. T.; Nguyen, S. T., Gas-Phase Dimerization of Ethylene under Mild Conditions Catalyzed by MOF Materials Containing (bpy)NiII Complexes. *ACS Catalysis* **2015**, *5* (11), 6713-6718.
95. Canivet, J.; Aguado, S.; Schuurman, Y.; Farrusseng, D., MOF-Supported Selective Ethylene Dimerization Single-Site Catalysts through One-Pot Postsynthetic Modification. *Journal of the American Chemical Society* **2013**, *135* (11), 4195-4198.
96. Ahn, S.; Nauert, S. L.; Hicks, K. E.; Ardagh, M. A.; Schweitzer, N. M.; Farha, O. K.; Notestein, J. M., Demonstrating the Critical Role of Solvation in Supported Ti and Nb Epoxidation Catalysts via Vapor-Phase Kinetics. *ACS Catalysis* **2020**, *10* (4), 2817-2825.
97. Neurock, M.; Manzer, L. E., Theoretical insights on the mechanism of alkene epoxidation by H₂O₂ with titanium silicalite. *Chemical Communications* **1996**, (10), 1133-1134.
98. Sever, R. R.; Root, T. W., DFT Study of Solvent Coordination Effects on Titanium-Based Epoxidation Catalysts. Part Two: Reactivity of Titanium Hydroperoxo Complexes in Ethylene Epoxidation. *The Journal of Physical Chemistry B* **2003**, *107* (17), 4090-4099.
99. Wan, H.; Vitter, A.; Chaudhari, R. V.; Subramaniam, B., Kinetic investigations of unusual solvent effects during Ru/C catalyzed hydrogenation of model oxygenates. *Journal of Catalysis* **2014**, *309*, 174-184.
100. Akpa, B. S.; D'Agostino, C.; Gladden, L. F.; Hindle, K.; Manyar, H.; McGregor, J.; Li, R.; Neurock, M.; Sinha, N.; Stitt, E. H.; Weber, D.; Zeitler, J. A.; Rooney, D. W., Solvent effects in the hydrogenation of 2-butanone. *Journal of Catalysis* **2012**, *289*, 30-41.
101. Zare, M.; Solomon, R. V.; Yang, W.; Yonge, A.; Heyden, A., Theoretical Investigation of Solvent Effects on the Hydrodeoxygenation of Propionic Acid over a Ni(111) Catalyst Model. *The Journal of Physical Chemistry C* **2020**, *124* (30), 16488-16500.
102. Mamun, O.; Saleheen, M.; Bond, J. Q.; Heyden, A., Investigation of solvent effects in the hydrodeoxygenation of levulinic acid to γ -valerolactone over Ru catalysts. *Journal of Catalysis* **2019**, *379*, 164-179.
103. Yang, W.; Solomon, R. V.; Lu, J.; Mamun, O.; Bond, J. Q.; Heyden, A., Unraveling the mechanism of the hydrodeoxygenation of propionic acid over a Pt (1 1 1) surface in vapor and liquid phases. *Journal of Catalysis* **2020**, *381*, 547-560.
104. Behtash, S.; Lu, J.; Mamun, O.; Williams, C. T.; Monnier, J. R.; Heyden, A., Solvation Effects in the Hydrodeoxygenation of Propanoic Acid over a Model Pd(211) Catalyst. *The Journal of Physical Chemistry C* **2016**, *120* (5), 2724-2736.
105. Behtash, S.; Lu, J.; Walker, E.; Mamun, O.; Heyden, A., Solvent effects in the liquid phase hydrodeoxygenation of methyl propionate over a Pd(111) catalyst model. *Journal of Catalysis* **2016**, *333*, 171-183.
106. Gould, N. S.; Xu, B., Temperature-Programmed Desorption of Pyridine on Zeolites in the Presence of Liquid Solvents. *ACS Catalysis* **2018**, *8* (9), 8699-8708.
107. Gould, N. S.; Li, S.; Cho, H. J.; Landfield, H.; Caratzoulas, S.; Vlachos, D.; Bai, P.; Xu, B., Understanding solvent effects on adsorption and protonation in porous catalysts. *Nature Communications* **2020**, *11* (1), 1060.
108. Bai, P.; Tsapatsis, M.; Siepmann, J. I., Multicomponent Adsorption of Alcohols onto Silicalite-1 from Aqueous Solution:

- Isotherms, Structural Analysis, and Assessment of Ideal Adsorbed Solution Theory. *Langmuir* **2012**, *28* (44), 15566-15576.
109. Wang, C.-H.; Bai, P.; Siepmann, J. I.; Clark, A. E., Deconstructing Hydrogen-Bond Networks in Confined Nanoporous Materials: Implications for Alcohol–Water Separation. *The Journal of Physical Chemistry C* **2014**, *118* (34), 19723-19732.
110. Dejaco, R. F.; Bai, P.; Tsapatsis, M.; Siepmann, J. I., Adsorptive Separation of 1-Butanol from Aqueous Solutions Using MFI- and FER-Type Zeolite Frameworks: A Monte Carlo Study. *Langmuir* **2016**, *32* (8), 2093-2101.
111. Krishna, R.; Van Baten, J. M., Hydrogen Bonding Effects in Adsorption of Water–Alcohol Mixtures in Zeolites and the Consequences for the Characteristics of the Maxwell–Stefan Diffusivities. *Langmuir* **2010**, *26* (13), 10854-10867.
112. Haque, E.; Jun, J. W.; Jhung, S. H., Adsorptive removal of methyl orange and methylene blue from aqueous solution with a metal-organic framework material, iron terephthalate (MOF-235). *Journal of Hazardous Materials* **2011**, *185* (1), 507-511.
113. Huo, S.-H.; Yan, X.-P., Metal–organic framework MIL-100(Fe) for the adsorption of malachite green from aqueous solution. *Journal of Materials Chemistry* **2012**, *22* (15), 7449.
114. Huang, Y.; Jiao, Y.; Chen, T.; Gong, Y.; Wang, S.; Liu, Y.; Sholl, D. S.; Walton, K. S., Tuning the Wettability of Metal–Organic Frameworks via Defect Engineering for Efficient Oil/Water Separation. *ACS Applied Materials & Interfaces* **2020**, *12* (30), 34413-34422.
115. Wright, A. M.; Rieth, A. J.; Yang, S.; Wang, E. N.; Dincă, M., Precise control of pore hydrophilicity enabled by post-synthetic cation exchange in metal–organic frameworks. *Chemical Science* **2018**, *9* (15), 3856-3859.
116. Rieth, A. J.; Wright, A. M.; Skorupskii, G.; Mancuso, J. L.; Hendon, C. H.; Dincă, M., Record-Setting Sorbents for Reversible Water Uptake by Systematic Anion Exchanges in Metal–Organic Frameworks. *Journal of the American Chemical Society* **2019**, *141* (35), 13858-13866.
117. Siegelman, R. L.; Milner, P. J.; Forse, A. C.; Lee, J.-H.; Colwell, K. A.; Neaton, J. B.; Reimer, J. A.; Weston, S. C.; Long, J. R., Water Enables Efficient CO₂ Capture from Natural Gas Flue Emissions in an Oxidation-Resistant Diamine-Appended Metal–Organic Framework. *Journal of the American Chemical Society* **2019**, *141* (33), 13171-13186.
118. Bodenschatz, C. J.; Sarupria, S.; Getman, R. B., Molecular-Level Details about Liquid H₂O Interactions with CO and Sugar Alcohol Adsorbates on Pt(111) Calculated Using Density Functional Theory and Molecular Dynamics. *The Journal of Physical Chemistry C* **2015**, *119* (24), 13642-13651.
119. Zhang, X.; Defever, R. S.; Sarupria, S.; Getman, R. B., Free Energies of Catalytic Species Adsorbed to Pt(111) Surfaces under Liquid Solvent Calculated Using Classical and Quantum Approaches. *Journal of Chemical Information and Modeling* **2019**, *59* (5), 2190-2198.
120. Yang, J.; Dauenhauer, P. J.; Ramasubramaniam, A., The role of water in the adsorption of oxygenated aromatics on Pt and Pd. *Journal of Computational Chemistry* **2013**, *34* (1), 60-66.
121. Yang, G.; Akhade, S. A.; Chen, X.; Liu, Y.; Lee, M.-S.; Glezakou, V.-A.; Rousseau, R.; Lercher, J. A., The Nature of Hydrogen Adsorption on Platinum in the Aqueous Phase. *Angewandte Chemie International Edition* **2019**, *58* (11), 3527-3532.
122. Abraham, M. H., Free energies, enthalpies, and entropies of solution of gaseous nonpolar nonelectrolytes in water and nonaqueous solvents. The hydrophobic effect. *Journal of the American Chemical Society* **1982**, *104* (8), 2085-2094.
123. Brønsted, J. N., Studies on Solubility. Iv. The Principle of the Specific Interaction of Ions. *Journal of the American Chemical Society* **1922**, *44* (5), 877-898.
124. Waeglele, M. M.; Gunathunge, C. M.; Li, J.; Li, X., How cations affect the electric double layer and the rates and selectivity of electrocatalytic processes. *The Journal of Chemical Physics* **2019**, *151* (16), 160902.
125. Choudhary, V.; Mushrif, S. H.; Ho, C.; Anderko, A.; Nikolakis, V.; Marinkovic, N. S.; Frenkel, A. I.; Sandler, S. I.; Vlachos, D. G., Insights into the Interplay of Lewis and Brønsted Acid Catalysts in Glucose and Fructose Conversion to 5-(Hydroxymethyl)furfural and Levulinic Acid in Aqueous Media. *Journal of the American Chemical Society* **2013**, *135* (10), 3997-4006.
126. Paolucci, C.; Di Iorio, J. R.; Schneider, W. F.; Gounder, R., Solvation and Mobilization of Copper Active Sites in Zeolites by Ammonia: Consequences for the Catalytic Reduction of Nitrogen Oxides. *Accounts of Chemical Research* **2020**, *53* (9), 1881-1892.
127. Enslow, K. R.; Bell, A. T., The Role of Metal Halides in Enhancing the Dehydration of Xylose to Furfural. *ChemCatChem* **2015**, *7* (3), 479-489.
128. Mushrif, S. H.; Varghese, J. J.; Vlachos, D. G., Insights into the Cr(III) catalyzed isomerization mechanism of glucose to fructose in the presence of water using ab initio molecular dynamics. *Physical Chemistry Chemical Physics* **2014**, *16* (36), 19564-19572.
129. Tang, J.; Guo, X.; Zhu, L.; Hu, C., Mechanistic Study of Glucose-to-Fructose Isomerization in Water Catalyzed by [Al(OH)₂(aq)]⁺. *ACS Catalysis* **2015**, *5* (9), 5097-5103.
130. Norton, A. M.; Nguyen, H.; Xiao, N. L.; Vlachos, D. G., Direct speciation methods to quantify catalytically active species of AlCl₃ in glucose isomerization. *RSC Advances* **2018**, *8* (31), 17101-17109.
131. Enslow, K. R.; Bell, A. T., SnCl₄-catalyzed isomerization/dehydration of xylose and glucose to furanics in water. *Catalysis Science & Technology* **2015**, *5* (5), 2839-2847.
132. Choudhary, V.; Pinar, A. B.; Lobo, R. F.; Vlachos, D. G.; Sandler, S. I., Comparison of Homogeneous and Heterogeneous Catalysts for Glucose-to-Fructose Isomerization in Aqueous Media. *ChemSusChem* **2013**, *6* (12), 2369-2376.
133. Paolucci, C.; Parekh, A. A.; Khurana, I.; Di Iorio, J. R.; Li, H.; Albarracin Caballero, J. D.; Shih, A. J.; Anggara, T.; Delgass, W. N.; Miller, J. T.; Ribeiro, F. H.; Gounder, R.; Schneider, W. F., Catalysis in a Cage: Condition-Dependent Speciation and Dynamics of Exchanged Cu Cations in SSZ-13 Zeolites. *Journal of the American Chemical Society* **2016**, *138* (18), 6028-6048.
134. Paolucci, C.; Khurana, I.; Parekh, A. A.; Li, S.; Shih, A. J.; Li, H.; Di Iorio, J. R.; Albarracin-Caballero, J. D.; Yezerets, A.; Miller, J. T.; Delgass, W. N.; Ribeiro, F. H.; Schneider, W. F.; Gounder, R., Dynamic multinuclear sites formed by mobilized copper ions in NO_xselective catalytic reduction. *Science* **2017**, *357* (6354), 898-903.
135. Resasco, J.; Chen, L. D.; Clark, E.; Tsai, C.; Hahn, C.; Jaramillo, T. F.; Chan, K.; Bell, A. T., Promoter Effects of Alkali Metal Cations on the Electrochemical Reduction of Carbon Dioxide. *Journal of the American Chemical Society* **2017**, *139* (32), 11277-11287.
136. Ringe, S.; Clark, E. L.; Resasco, J.; Walton, A.; Seger, B.; Bell, A. T.; Chan, K., Understanding cation effects in electrochemical CO₂ reduction. *Energy & Environmental Science* **2019**, *12* (10), 3001-3014.
137. Gunathunge, C. M.; Ovalle, V. J.; Waeglele, M. M., Probing promoting effects of alkali cations on the reduction of CO at the aqueous electrolyte/copper interface. *Physical Chemistry Chemical Physics* **2017**, *19* (44), 30166-30172.
138. Li, J.; Wu, D.; Malkani, A. S.; Chang, X.; Cheng, M. J.; Xu, B.; Lu, Q., Hydroxide Is Not a Promoter of C₂₊ Product Formation in the

- Electrochemical Reduction of CO on Copper. *Angewandte Chemie International Edition* **2020**, *59* (11), 4464-4469.
139. Li, J.; Li, X.; Gunathunge, C. M.; Waegle, M. M., Hydrogen bonding steers the product selectivity of electrocatalytic CO reduction. *Proceedings of the National Academy of Sciences* **2019**, *116* (19), 9220-9229.
140. Gilkey, M. J.; Xu, B., Heterogeneous Catalytic Transfer Hydrogenation as an Effective Pathway in Biomass Upgrading. *ACS Catalysis* **2016**, *6* (3), 1420-1436.
141. Kulkarni, N. V.; Brennessel, W. W.; Jones, W. D., Catalytic Upgrading of Ethanol to n-Butanol via Manganese-Mediated Guerbet Reaction. *ACS Catalysis* **2018**, *8* (2), 997-1002.
142. Aitchison, H.; Wingad, R. L.; Wass, D. F., Homogeneous Ethanol to Butanol Catalysis—Guerbet Renewed. *ACS Catalysis* **2016**, *6* (10), 7125-7132.
143. Li, W.; Su, M.; Zhang, T.; Ma, Q.; Fan, W., Production of liquid fuel intermediates from furfural via aldol condensation over potassium-promoted Sn-MFI catalyst. *Fuel* **2019**, *237*, 1281-1290.
144. Müller, P.; Burt, S. P.; Love, A. M.; McDermott, W. P.; Wolf, P.; Hermans, I., Mechanistic Study on the Lewis Acid Catalyzed Synthesis of 1,3-Butadiene over Ta-BEA Using Modulated Operando DRIFTS-MS. *ACS Catalysis* **2016**, *6* (10), 6823-6832.
145. Jessop, P. G.; Ikariya, T.; Noyori, R., Homogeneous Catalysis in Supercritical Fluids. *Chemical Reviews* **1999**, *99* (2), 475-494.
146. Jessop, P. G.; Ikariya, T.; Noyori, R., Homogeneous catalytic hydrogenation of supercritical carbon dioxide. *Nature* **1994**, *368* (6468), 231-233.
147. Jessop, P. G., Homogeneously-catalyzed syntheses in supercritical fluids. *Topics In Catalysis* **1998**, *5* (1/4), 95-103.
148. Jiang, J.-L.; Gao, F.; Hua, R.; Qiu, X., Re(CO)₅Br-Catalyzed Coupling of Epoxides with CO₂Affording Cyclic Carbonates under Solvent-Free Conditions. *The Journal of Organic Chemistry* **2005**, *70* (1), 381-383.
149. Mang, S.; Cooper, A. I.; Colclough, M. E.; Chauhan, N.; Holmes, A. B., Copolymerization of CO₂ and 1,2-Cyclohexene Oxide Using a CO₂-Soluble Chromium Porphyrin Catalyst. *Macromolecules* **2000**, *33* (2), 303-308.
150. Panagiotopoulou, P.; Martin, N.; Vlachos, D. G., Effect of hydrogen donor on liquid phase catalytic transfer hydrogenation of furfural over a Ru/RuO₂/C catalyst. *Journal of Molecular Catalysis A: Chemical* **2014**, *392*, 223-228.
151. Scholz, D.; Aellig, C.; Hermans, I., Catalytic Transfer Hydrogenation/Hydrogenolysis for Reductive Upgrading of Furfural and 5-(Hydroxymethyl)furfural. *ChemSusChem* **2014**, *7* (1), 268-275.
152. Lewis, J. D.; Van De Vyver, S.; Crisci, A. J.; Gunther, W. R.; Michaelis, V. K.; Griffin, R. G.; Román-Leshkov, Y., A Continuous Flow Strategy for the Coupled Transfer Hydrogenation and Etherification of 5-(Hydroxymethyl)furfural using Lewis Acid Zeolites. *ChemSusChem* **2014**, *7* (8), 2255-2265.
153. Tang, X.; Zeng, X.; Li, Z.; Li, W.; Jiang, Y.; Hu, L.; Liu, S.; Sun, Y.; Lin, L., In Situ Generated Catalyst System to Convert Biomass-Derived Levulinic Acid to γ -Valerolactone. *ChemCatChem* **2015**, *7* (8), 1372-1379.
154. Luo, H. Y.; Consoli, D. F.; Gunther, W. R.; Román-Leshkov, Y., Investigation of the reaction kinetics of isolated Lewis acid sites in Beta zeolites for the Meerwein-Ponndorf-Verley reduction of methyl levulinate to γ -valerolactone. *Journal of Catalysis* **2014**, *320*, 198-207.
155. Yang, Z.; Huang, Y.-B.; Guo, Q.-X.; Fu, Y., RANEY® Ni catalyzed transfer hydrogenation of levulinate esters to γ -valerolactone at room temperature. *Chemical Communications* **2013**, *49* (46), 5328-5330.
156. Chia, M.; Dumesic, J. A., Liquid-phase catalytic transfer hydrogenation and cyclization of levulinic acid and its esters to γ -valerolactone over metal oxide catalysts. *Chemical Communications* **2011**, *47* (44), 12233-12235.
157. Reece, S. Y.; Nocera, D. G., Proton-Coupled Electron Transfer in Biology: Results from Synergistic Studies in Natural and Model Systems. *Annual Review of Biochemistry* **2009**, *78* (1), 673-699.
158. Pannwitz, A.; Wenger, O. S., Recent advances in bioinspired proton-coupled electron transfer. *Dalton Transactions* **2019**, *48* (18), 5861-5868.
159. Huynh, M. H. V.; Meyer, T. J., Proton-Coupled Electron Transfer. *Chemical Reviews* **2007**, *107* (11), 5004-5064.
160. Bard, A. J.; Faulkner, L. R., *Electrochemical methods and applications*. Wiley-Interscience: New York; London, 2000.
161. Haruta, M.; Kobayashi, T.; Sano, H.; Yamada, N., Novel Gold Catalysts for the Oxidation of Carbon Monoxide at a Temperature far Below 0 °C. *Chemistry Letters* **1987**, *16* (2), 405-408.
162. Cunningham, D. A. H.; Vogel, W.; Haruta, M., Negative activation energies in CO oxidation over an icosahedral Au/Mg(OH)₂ catalyst. *Catalysis Letters* **1999**, *63*, 43-47.
163. Daté, M.; Haruta, M., Moisture Effect on CO Oxidation over Au/TiO₂ Catalyst. *Journal of Catalysis* **2001**, *201* (2), 221-224.
164. Daté, M.; Okumura, M.; Tsubota, S.; Haruta, M., Vital Role of Moisture in the Catalytic Activity of Supported Gold Nanoparticles. *Angewandte Chemie International Edition* **2004**, *43* (16), 2129-2132.
165. Haruta, M.; Takase, T.; Kobayashi, T., In *Catalytic Science and Technology*, Yoshida, S.; Takezawa, N.; Ono, T., Eds. Kodansha: Tokyo, 1991; Vol. 1, pp 331-334.
166. Desai, S.; Neurock, M., A first principles analysis of CO oxidation over Pt and Pt66.7%Ru33.3% (111) surfaces. *Electrochimica Acta* **2003**, *48* (25-26), 3759-3773.
167. Desai, S. K.; Neurock, M., First-principles study of the role of solvent in the dissociation of water over a Pt-Ru alloy. *Physical Review B* **2003**, *68* (7).
168. Saavedra, J.; Doan, H. A.; Pursell, C. J.; Grabow, L. C.; Chandler, B. D., The critical role of water at the gold-titania interface in catalytic CO oxidation. *Science* **2014**, *345* (6204), 1599-1602.
169. Saavedra, J.; Whittaker, T.; Chen, Z.; Pursell, C. J.; Rioux, R. M.; Chandler, B. D., Controlling activity and selectivity using water in the Au-catalysed preferential oxidation of CO in H₂. *Nature Chemistry* **2016**, *8* (6), 584-589.
170. Saavedra, J.; Pursell, C. J.; Chandler, B. D., CO Oxidation Kinetics over Au/TiO₂ and Au/Al₂O₃ Catalysts: Evidence for a Common Water-Assisted Mechanism. *Journal of the American Chemical Society* **2018**, *140* (10), 3712-3723.
171. Ojeda, M.; Zhan, B.-Z.; Iglesia, E., Mechanistic interpretation of CO oxidation turnover rates on supported Au clusters. *Journal of Catalysis* **2012**, *285* (1), 92-102.
172. Zope, B. N.; Hibbitts, D. D.; Neurock, M.; Davis, R. J., Reactivity of the Gold/Water Interface During Selective Oxidation Catalysis. *Science* **2010**, *330* (6000), 74-78.
173. Ide, M. S.; Davis, R. J., The Important Role of Hydroxyl on Oxidation Catalysis by Gold Nanoparticles. *Accounts of Chemical Research* **2014**, *47* (3), 825-833.
174. Hensley, A. J. R.; Wang, Y.; Mei, D.; McEwen, J.-S., Mechanistic Effects of Water on the Fe-Catalyzed Hydrodeoxygenation of Phenol. The Role of Brønsted Acid Sites. *ACS Catalysis* **2018**, 2200-2208.
175. Nelson, R. C.; Baek, B.; Ruiz, P.; Goundie, B.; Brooks, A.; Wheeler, M. C.; Frederick, B. G.; Grabow, L. C.; Austin, R. N., Experimental and Theoretical Insights into the Hydrogen-Efficient

- Direct Hydrodeoxygenation Mechanism of Phenol over Ru/TiO₂. *ACS Catalysis* **2015**, *5* (11), 6509–6523.
176. Omotoso, T. O.; Baek, B.; Grabow, L. C.; Crossley, S. P., Experimental and First-Principles Evidence for Interfacial Activity of Ru/TiO₂ for the Direct Conversion of *m*-Cresol to Toluene. *ChemCatChem* **2017**, *9* (14), 2642–2651.
177. Wilson, N. M.; Flaherty, D. W., Mechanism for the Direct Synthesis of H₂O₂ on Pd Clusters: Heterolytic Reaction Pathways at the Liquid–Solid Interface. *Journal of the American Chemical Society* **2016**, *138* (2), 574–586.
178. Wilson, N. M.; Schröder, J.; Priyadarshini, P.; Bregante, D. T.; Kunz, S.; Flaherty, D. W., Direct synthesis of H₂O₂ on PdZn nanoparticles: The impact of electronic modifications and heterogeneity of active sites. *Journal of Catalysis* **2018**, *368*, 261–274.
179. Wilson, N. M.; Priyadarshini, P.; Kunz, S.; Flaherty, D. W., Direct synthesis of H₂O₂ on Pd and AuPd₁ clusters: Understanding the effects of alloying Pd with Au. *Journal of Catalysis* **2018**, *357*, 163–175.
180. Adams, J. S.; Chemburkar, A.; Priyadarshini, P.; Ricciardulli, T.; Lu, Y.; Maliekkal, V.; Sampath, A.; Winikoff, S.; Karim, A. M.; Neurock, M.; Flaherty, D. W., Solvent molecules form surface redox mediators in situ and cocatalyze O₂ reduction on Pd. *Science* **2021**, *371*, 626–632.
181. Wilson, N. M.; Pan, Y.-T.; Shao, Y.-T.; Zuo, J.-M.; Yang, H.; Flaherty, D. W., Direct Synthesis of H₂O₂ on AgPt Octahedra: The Importance of Ag–Pt Coordination for High H₂O₂ Selectivity. *ACS Catalysis* **2018**, *8* (4), 2880–2889.
182. Ricciardulli, T.; Gorthy, S.; Adams, J. S.; Thompson, C.; Karim, A. M.; Neurock, M.; Flaherty, D. W., Effect of Pd Coordination and Isolation on the Catalytic Reduction of O₂ to H₂O₂ over PdAu Bimetallic Nanoparticles. *Journal of the American Chemical Society* **2021**, *143* (14), 5445–5464.
183. Adams, J. S.; Kromer, M. L.; Rodríguez-López, J.; Flaherty, D. W., Unifying Concepts in Electro- and Thermocatalysis toward Hydrogen Peroxide Production. *Journal of the American Chemical Society* **2021**, *143* (21), 7940–7957.
184. Cai, H.; Schimmenti, R.; Nie, H.; Mavrikakis, M.; Chin, Y.-H. C., Mechanistic Role of the Proton–Hydride Pair in Heteroarene Catalytic Hydrogenation. *ACS Catalysis* **2019**, *9* (10), 9418–9437.
185. Campos-Roldán, C. A.; Alonso-Vante, N., The Hydrogen Oxidation Reaction in Alkaline Medium: An Overview. *Electrochemical Energy Reviews* **2019**, *2* (2), 312–331.
186. Zheng, J.; Sheng, W.; Zhuang, Z.; Xu, B.; Yan, Y., Universal dependence of hydrogen oxidation and evolution reaction activity of platinum-group metals on pH and hydrogen binding energy. *Science Advances* **2016**, *2* (3), e1501602.
187. Davydova, E. S.; Mukerjee, S.; Jaouen, F.; Dekel, D. R., Electrocatalysts for Hydrogen Oxidation Reaction in Alkaline Electrolytes. *ACS Catalysis* **2018**, *8* (7), 6665–6690.
188. Whittaker, T.; Kumar, K. B. S.; Peterson, C.; Pollock, M. N.; Grabow, L. C.; Chandler, B. D., H₂ Oxidation over Supported Au Nanoparticle Catalysts: Evidence for Heterolytic H₂ Activation at the Metal–Support Interface. *Journal of the American Chemical Society* **2018**, *140* (48), 16469–16487.
189. Srajan Kumar, K. B.; Whittaker, T. N.; Peterson, C.; Grabow, L. C.; Chandler, B. D., Water Poisons H₂ Activation at the Au–TiO₂ Interface by Slowing Proton and Electron Transfer between Au and Titania. *Journal of the American Chemical Society* **2020**, *142* (12), 5760–5772.
190. Mahdavi-Shakib, A.; Kumar, K. B. S.; Whittaker, T. N.; Xie, T.; Grabow, L. C.; Rioux, R. M.; Chandler, B. D., Kinetics of H₂ Adsorption at the Metal–Support Interface of Au/TiO₂ Catalysts Probed by Broad Background IR Absorbance. *Angewandte Chemie* **2021**, *133* (14), 7814–7822.
191. Shangguan, J.; Olarte, M. V.; Chin, Y.-H., Mechanistic insights on CO and CC bond activation and hydrogen insertion during acetic acid hydrogenation catalyzed by ruthenium clusters in aqueous medium. *Journal of Catalysis* **2016**, *340*, 107–121.
192. Shangguan, J.; Chin, Y.-H. C., Kinetic Significance of Proton–Electron Transfer during Condensed Phase Reduction of Carbonyls on Transition Metal Clusters. *ACS Catalysis* **2019**, 1763–1778.
193. Shangguan, J.; Hensley, A. J. R.; Gradiski, M. V.; Pfriem, N.; McEwen, J.-S.; Morris, R. H.; Chin, Y.-H. C., The Role of Protons and Hydrides in the Catalytic Hydrogenolysis of Guaiacol at the Ruthenium Nanoparticle–Water Interface. *ACS Catalysis* **2020**, *10* (20), 12310–12332.
194. Zhao, Z.; Bababik, R.; Xue, W.; Li, Y.; Briggs, N. M.; Nguyen, D.-T.; Nguyen, U.; Crossley, S. P.; Wang, S.; Wang, B.; Resasco, D. E., Solvent-mediated charge separation drives alternative hydrogenation path of furanics in liquid water. *Nature Catalysis* **2019**, *2* (5), 431–436.
195. Hibbitts, D. D.; Loveless, B. T.; Neurock, M.; Iglesia, E., Mechanistic role of water on the rate and selectivity of Fischer–Tropsch synthesis on ruthenium catalysts. *Angewandte Chemie International Edition* **2013**, *52* (47), 12273–12278.
196. Hensley, A. J. R.; Bray, J.; Shangguan, J.; Chin, Y.-H.; McEwen, J.-S., Catalytic consequences of hydrogen addition events and solvent-adsorbate interactions during guaiacol–H₂ reactions at the H₂O–Ru(0 0 0 1) interface. *Journal of Catalysis* **2021**, *395*, 467–482.
197. Tran, H.-V.; Doan, H. A.; Chandler, B. D.; Grabow, L. C., Water-assisted oxygen activation during selective oxidation reactions. *Current Opinion in Chemical Engineering* **2016**, *13*, 100–108.
198. Hibbitts, D. D.; Neurock, M., Influence of oxygen and pH on the selective oxidation of ethanol on Pd catalysts. *Journal of Catalysis* **2013**, *299*, 261–271.
199. Hibbitts, D.; Neurock, M., Promotional effects of chemisorbed oxygen and hydroxide in the activation of C–H and O–H bonds over transition metal surfaces. *Surface Science* **2016**, *650*, 210–220.
200. Desai, S. K.; Pallassana, V.; Neurock, M., A Periodic Density Functional Theory Analysis of the Effect of Water Molecules on Deprotonation of Acetic Acid over Pd(111). *The Journal of Physical Chemistry B* **2001**, *105* (38), 9171–9182.
201. Augustine, R. L.; Warner, R. W.; Melnick, M. J., Heterogeneous catalysis in organic chemistry. 3. Competitive adsorption of solvents during alkene hydrogenations. *The Journal of Organic Chemistry* **1984**, *49* (25), 4853–4856.
202. Kishida, S., Kinetics of liquid-phase hydrogenation of acetone over Raney nickel catalyst. *Journal of Catalysis* **1968**, *12* (1), 90–96.
203. Clement, G. E.; Bender, M. L., The Effect of Aprotic Dipolar Organic Solvents on the Kinetics of α -Chymotrypsin-Catalyzed Hydrolyses *. *Biochemistry* **1963**, *2* (4), 836–843.
204. Gileadi, E.; Stoner, G. E., The Effect of Competition with Water on the Kinetic Parameters in Electrode Reactions. *Journal of The Electrochemical Society* **1971**, *118* (8), 1316–1319.
205. Takagi, H.; Isoda, T.; Kusakabe, K.; Morooka, S., Effects of Solvents on the Hydrogenation of Mono-Aromatic Compounds Using Noble-Metal Catalysts. *Energy & Fuels* **1999**, *13* (6), 1191–1196.
206. Rajadhyaksha, R. A.; Karwa, S. L., Solvent effects in catalytic hydrogenation. *Chemical Engineering Science* **1986**, *41* (7), 1765–1770.
207. Bregante, D. T.; Patel, A. Y.; Johnson, A. M.; Flaherty, D. W., Catalytic thiophene oxidation by groups 4 and 5 framework-substituted zeolites with hydrogen peroxide: Mechanistic and

spectroscopic evidence for the effects of metal Lewis acidity and solvent Lewis basicity. *Journal of Catalysis* **2018**, *364*, 415-425.

208. Müller, P.; Wolf, P.; Hermans, I., Insights into the Complexity of Heterogeneous Liquid-Phase Catalysis: Case Study on the Cyclization of Citronellal. *ACS Catalysis* **2016**, *6* (5), 2760-2769.

209. Akinola, J.; Barth, I.; Goldsmith, B. R.; Singh, N., Adsorption Energies of Oxygenated Aromatics and Organics on Rhodium and Platinum in Aqueous Phase. *ACS Catalysis* **2020**, *10* (9), 4929-4941.

210. Singh, N.; Campbell, C. T., A Simple Bond-Additivity Model Explains Large Decreases in Heats of Adsorption in Solvents Versus Gas Phase: A Case Study with Phenol on Pt(111) in Water. *ACS Catalysis* **2019**, *9* (9), 8116-8127.

211. He, J.; Zhao, C.; Lercher, J. A., Impact of solvent for individual steps of phenol hydrodeoxygenation with Pd/C and HZSM-5 as catalysts. *Journal of Catalysis* **2014**, *309*, 362-375.

212. Van Der Graaff, W. N. P.; Tempelman, C. H. L.; Li, G.; Mezari, B.; Kosinov, N.; Pidko, E. A.; Hensen, E. J. M., Competitive Adsorption of Substrate and Solvent in Sn-Beta Zeolite During Sugar Isomerization. *ChemSusChem* **2016**, *9* (22), 3145-3149.

213. Lide, D. R., *CRC handbook of chemistry and physics*. CRC press: 2004; Vol. 85.

214. Kwon, S.; Schweitzer, N. M.; Park, S.; Stair, P. C.; Snurr, R. Q., A kinetic study of vapor-phase cyclohexene epoxidation by H₂O₂ over mesoporous TS-1. *Journal of Catalysis* **2015**, *326*, 107-115.

215. Bates, J. S.; Gounder, R., Influence of confining environment polarity on ethanol dehydration catalysis by Lewis acid zeolites. *Journal of Catalysis* **2018**, *365*, 213-226.

216. Bukowski, B. C.; Bates, J. S.; Gounder, R.; Greeley, J., First principles, microkinetic, and experimental analysis of Lewis acid site speciation during ethanol dehydration on Sn-Beta zeolites. *Journal of Catalysis* **2018**, *365*, 261-276.

217. Zhi, Y.; Shi, H.; Mu, L.; Liu, Y.; Mei, D.; Camaioni, D. M.; Lercher, J. A., Dehydration Pathways of 1-Propanol on HZSM-5 in the Presence and Absence of Water. *Journal of the American Chemical Society* **2015**, *137* (50), 15781-15794.

218. Murphy, B. M.; Mou, T.; Wang, B.; Xu, B., The Effect of Cofed Species on the Kinetics of Catalytic Methyl Lactate Dehydration on NaY. *ACS Catalysis* **2018**, 9066-9078.

219. Di Iorio, J. R.; Hoffman, A. J.; Nimlos, C. T.; Nystrom, S.; Hibbitts, D.; Gounder, R., Mechanistic origins of the high-pressure inhibition of methanol dehydration rates in small-pore acidic zeolites. *Journal of Catalysis* **2019**, *380*, 161-177.

220. Clarke, C. J.; Tu, W.-C.; Levers, O.; Bröhl, A.; Hallett, J. P., Green and Sustainable Solvents in Chemical Processes. *Chemical Reviews* **2018**, *118* (2), 747-800.